ASCE

Consequence-Oriented Fire Intensity Optimization for Structural Design under Uncertainty

Andrea Franchini, S.M.ASCE[1]; Carmine Galasso, A.M.ASCE[2]; and Jose L. Torero[3]

Abstract: The first step in current methodologies for the (probabilistic) performance-based fire safety design and assessment of structures is characterizing fire hazard scenario(s). Next, structural response analysis is performed to estimate hazard consequences in terms of damage or loss metrics of interest. These metrics are eventually appraised to verify whether various performance objectives are achieved and design iterations are needed. Nevertheless, such approaches rely on preliminary assumptions on the structural configuration and features characterizing scenarios used as thermal inputs. Consequently, they do not fully exploit the fire–structure coupling effect, where fire affects a structure, and the characteristics of the structure also affect the combustion process and fire dynamics. Indeed, the structural design choices define the fire scenarios that could potentially affect the structural and nonstructural performance. This paper introduces a consequence-oriented fire intensity optimization (CFO) approach to the fire safety design of structures to address such limitations. The proposed approach considers fire scenarios as additional design variables and delivers them as procedure outputs, optimizing the balance between increasing structural capacity and decreasing fire intensity. Furthermore, it evaluates the effect of input uncertainties through Monte Carlo sampling. A single-span bridge subject to a car fire is used to showcase the proposed approach. For this case study, it is shown that fire scenario characteristics (fuel bed and traffic load positions, heat release rate history) maximizing consequences are strongly correlated to the structural features and cannot be set a priori. Finally, design decisions exploiting the described coupling effect to achieve various performance objectives are discussed. Overall, the proposed approach highlights the benefits of enhancing the fire and heat transfer model's capability to capture the fire–structure coupling effect for achieving more optimized design solutions. **DOI: 10.1061/JSENDH.STENG-12645.**

Introduction

Performance-Based Fire Safety Engineering

Major fire accidents in the built environment cause billions of dollars in economic losses and hundreds to thousands of casualties every year (e.g., Ahrens 2021; Brushlinsky et al. 2022; Clark 2023). Such events threaten different types of civil infrastructure systems, including buildings (e.g., Kodur et al. 2020), bridges (e.g., Hu et al. 2021), and tunnels (e.g., Kodur and Naser 2021). Currently, fire safety is tackled through fire safety strategies, which consist of several holistically interacting components (e.g., Lange et al. 2021): detection, warning, evacuation, smoke management, structural integrity management, and fire brigade intervention. Many countries have moved from prescriptive to performance-based fire design codes, facilitating any fire safety strategy that can achieve target performance objectives (e.g., Buchanan and Abu 2017; Hurley and Rosenbaum 2016). From the structural design perspective, performance-based engineering (PBE) quantifies and assesses performance in terms of consequences such as structural/nonstructural damage, repair costs, downtime, and casualty rates at selected levels of hazard intensity (e.g., Porter 2003).

In PBE, analysis and design approaches can be grouped into deterministic, semiprobabilistic, or fully probabilistic according to the uncertainty treatment they implement. Uncertain (random) variables in structural design include material properties, member geometry, mechanical models, and loads. Deterministic methods rely on conservative assumptions in performance quantification. Furthermore, they assess compliance with safety performance objectives through acceptance criteria often based on expert opinion and current practice (e.g., Van Coile et al. 2019). Semiprobabilistic approaches [e.g., load and resistance factor design (LRFD)] still involve deterministic analyses. However, they account for the probabilistic nature of the considered random variables through partial safety factors. Such factors (which aim to achieve a desired—conventional—safety level in structural cross sections/components) are applied to statistics of the random variables (mean or nominal values) or directly to measures of resistance and load effects (e.g., Iervolino and Galasso 2012). Van Coile et al. (2019) discussed that generally accepted semiprobabilistic fire safety design methodologies are still unavailable. Consistently, the Eurocodes for structural fire design [e.g., EN 1992-1-2 (CEN 2004a) for concrete, EN 1993-1-2 (CEN 2005b) for steel, EN 1995-1-2 (CEN 2004b) for timber] recommend using safety factors equal to 1.

A well-established PBE approach was developed by the Pacific Earthquake Engineering Research (PEER) center (Porter 2003; Mackie and Stojadinovic 2004; Moehle and Deierlein 2004) in the context of earthquake engineering. The PEER framework was then adapted and extended to other hazards such as wind (Petrini and Ciampoli 2012) [including hurricanes (Barbato et al. 2013)], tsunamis (Attary et al. 2017), and blasts (Whittaker et al. 2003). Several researchers also attempted to adapt the framework to design

[1]Ph.D. Student, Dept. of Civil, Environmental and Geomatic Engineering, Univ. College London, London WC1E 6BT, UK (corresponding author). ORCID: https://orcid.org/0000-0001-9732-2484. Email: andrea.franchini.19@ucl.ac.uk

[2]Professor, Dept. of Civil, Environmental and Geomatic Engineering, Univ. College London, London WC1E 6BT, UK. ORCID: https://orcid.org/0000-0001-5445-4911. Email: c.galasso@ucl.ac.uk

[3]Professor, Dept. of Civil, Environmental and Geomatic Engineering, Univ. College London, London WC1E 6BT, UK. Email: j.torero@ucl.ac.uk

Note. This manuscript was submitted on April 3, 2023; approved on September 21, 2023; published online on January 27, 2024. Discussion period open until June 27, 2024; separate discussions must be submitted for individual papers. This paper is part of the ***Journal of Structural Engineering***, © ASCE, ISSN 0733-9445.

fire-resistant structures (e.g., Lange et al. 2014; Gernay et al. 2016; Ma et al. 2019). A review of research advances and perspectives on the topic is provided by Shrivastava et al. (2019).

The described approaches can be used to assess existing structures or design new structures. An assessment tests an existing structure's adequacy in terms of target performance objectives described by specific consequence metrics. Conversely, the design process aims at selecting design variables that comply with (design for compliance) or optimize (design optimization) the target performance objectives. The focus of this paper is PBE for design purposes.

A Structure-Specific Hazard

Like design practices for other extreme events, PBE approaches to fire safety design commonly start by drawing assumptions on the structural configuration and features characterizing scenarios used as thermal inputs. Next, they assess structural response and use the results to estimate fire consequences in terms of damage or loss metrics of interest. Finally, if the considered performance objectives (in terms of the consequence metrics of interest) are not achieved, the structural design is updated, and the performance is iteratively checked against those preset hazard scenarios. This workflow, however, is suitable for site-specific hazards, i.e., those whose effect does not depend (or weakly depend) on the considered structure's features but rather on its location (e.g., wind, earthquake). In such circumstances, the intensity of the hazard can be modeled probabilistically to account for aleatory uncertainties induced by natural variability.

On the other hand, in the case of a fire, the governing probabilistic variable is the fuel load. Nevertheless, the structural performance is governed by the temperature distribution within all structural system elements. The temperature evolution in time is determined by cross-sectional design variables and the thermal boundary condition (i.e., surface heat flux). Furthermore, the evolution of the heat flux is defined by the nature of the fire, which is strongly coupled with the structural features and thermal/thermomechanical response of the structure.

Indeed, differently from all the other hazards, fire is a hazard that evolves in space and time as a function of the structure in which it develops. In this process, structural and fire behaviors are dynamically coupled, resulting in a feedback loop (denoted as *fire–structure coupling effect* in this paper) by which the fire affects the structure as much as the structure modifies fire behavior (Torero 2006, 2013b). In this definition of fire–structure coupling effect, we include the structure in a holistic manner, comprising structural elements such as beams, columns, trusses, and slabs; the nonstructural components these elements support; thermal properties of the boundaries; and openings, ceiling height, global dimensions, and geometry of the volume (in the case of compartment and tunnel fires). This broader definition also acknowledges that alterations to nonstructural elements, such as their materials, ceiling height, or volume geometry, may necessitate corresponding modifications to the structural components. The fire-structure coupling effect appears as follows:

- Fire is an exothermic combustion reaction. The process is driven by buoyancy but is affected by the geometry of the fuel and surrounding structure. Fuel characteristics and surroundings determine the flame location and geometry (e.g., Drysdale 2011; Torero 2013a).
- The fire releases energy and species through mass and heat fluxes. These fluxes intensively interact with the surroundings (e.g., Karlsson and Quintiere 2022) and heat structural and nonstructural elements, changing material properties and geometrical features.
- Heated structural and nonstructural elements radiate energy back to the fuel bed [radiative feedback (Torero 2013b)], affecting the combustion process and providing energy that influences the buoyancy-driven gas flows (Torero 2013a). Furthermore, the radiant heat from heated surfaces can ignite other combustible items (e.g., Drysdale 2011).
- Some structural elements (e.g., concrete slabs) might be exploited as heat sinks, reducing the heat feedback effect and the heat flux to other structural elements.
- Finally, the duration of the fire is determined by the amount of combustible materials (fuel load) and the burning rate. The burning rate is controlled by the characteristics of the combustion process and, therefore, by all the variables that affect the combustion process.

Modeling some other hazards (e.g., wind and flood) also requires considering load–structure interaction. For example, in the probabilistic performance-based wind engineering framework (Petrini and Ciampoli 2012), site- and structure-specific hazard analyses precede structural analysis. Here, structure-specific analysis refers to aerodynamic analysis and provides a set of interaction parameters affecting the structural response. However, this response also depends on the site-specific probabilistic model of the wind velocity field. Hence, in the context of this paper, wind and flood can still be considered site-specific hazards, as discussed previously.

Several references in the literature investigated the fire–structure coupling effect, identifying the problem geometry (layout and shape of structural and nonstructural elements, fuel location) and the material properties as critical factors. For example, Gritzo and Nicolette (1997) found that the fire phenomenon is strongly coupled with the size, shape, location, orientation, and thermal response of engulfed or nearby objects. The authors of that study identified two coupling modes (radiative and convective) and showed that modifying the listed parameters significantly affects the heat flux to the object. In response, heat flux variations alter the object's thermal response and geometry.

The geometry also significantly affects radiation, the mechanism through which the hot layer and structural and nonstructural components transfer energy back to the fuel bed (Drysdale 2011). Indeed, this mechanism depends on configuration factors describing the geometrical relationship between the emitter and the receiver (e.g., Buchanan and Abu 2017; Drysdale 2011), implying that different geometrical configurations modify the fire growth and the thermomechanical response. In a compartment fire, the gas phase temperature at the steady-state condition is dictated by the enclosure geometry, characterized by dimensions, aspect ratio, and openings (Torero et al. 2014). Moreover, the building layout affects fire and smoke spread, occupant evacuation, and firefighter access (Hadjisophocleous and Mehaffey 2016).

Another critical design decision affecting the fire–structure coupling effect is the choice of materials for the elements surrounding the fire. For instance, considering compartment fires, it is well understood from early studies (e.g., Kawagoe 1958; Thomas et al. 1967) and more recent works (e.g., Torero et al. 2014, 2017) that the thermal properties of the enclosure surface strongly affect the energy balance, fire development, and gas temperatures. Furthermore, during the fire decay phase, the decay rate depends on the solid phase (construction materials) cooling rather than the gas phase cooling (Khan et al. 2021). This consideration is essential when assessing the possibility of delayed failure, i.e., the structural failure occurring after the maximum fire temperature (Gernay and Salah Dimia 2013). The choice of different materials also implies different mechanical properties, structural member forms, and interaction mechanisms that unequivocally yield differing structural responses and failure mechanisms.

Evidence of the fire–structure coupling effect also comes from the observation that heat release rates (HRRs), ignitability, and flame spread depend on both the physical/chemical nature of the burning substance and the heating boundary conditions (Babrauskas 2016).

Accordingly, the mass loss rate measured in the Valencia bridge test (Alos-Moya et al. 2017) increased when moving the fuel pan closer to the bridge deck (due to increased heat feedback). Still, it decreased when moving the pan close to the abutment (because of the reduced ventilation). Other studies showed that the heat feedback to the fuel depends on (1) flame volume, fuel location, and bridge geometry for bridges (Peris-Sayol et al. 2016); and (2) lining type, cross-sectional area, ventilation, and flame volume for tunnels (Ingason et al. 1994).

A particular case of strong coupling between structures and fire is that of timber (or, more generally, combustible) materials/structures that ignite and contribute to the fuel (e.g., Buchanan and Abu 2017). The rate at which fire spreads through timber structures depends on factors such as ventilation, fuel load, and the presence of openings. At the same time, charring forms a protective layer that slows the rate of combustion.

People's response (e.g., evacuation, use of fire extinguishers) and countermeasures (e.g., sprinklers) also affect the fire–structure coupling effect, emphasizing that fire safety can only be quantified if the combustion process and fire dynamics are assessed in the context of their environment (Torero 2013a).

It is noted that a designer's ability to exploit the fire–structure coupling effect relies on two factors: (1) the model's capability to capture the fire–structure coupling effect; and (2) the degree of coupling between the considered members and the fire. In situations where the coupling is weak, the potential design benefits, even if they exist, may not outweigh the complexities introduced by the modeling process. This consideration becomes particularly relevant when computational fluid dynamics (CFD) models are required for fire–structure coupling modeling. In this regard, Charlier et al. (2021) advised that structural elements should be considered only if they form a compartment boundary (e.g., walls and slabs) or if they significantly influence mass and radiative flows (e.g., deep concrete beams, wide columns). Similarly, Tondini et al. (2016) suggested that weak coupling (i.e., lack of mutual interaction among fire development, element thermal, and mechanical response) might be assumed for structures of thin members in large compartments.

Scope

The previous discussion demonstrates that (structural) design decisions regarding geometry, materials, and fire safety strategy determine the fire growth, spread, and decay, making fire a structure-specific hazard. In other words, the selected design defines the hazard's intensity, demanding the joint estimation of fire scenarios and structural features. In this sense, proper structural optimization should address structural and fire behavior in a coupled manner (Torero 2013b). Conversely, developing the design starting from the hazard preliminarily constrains the design choices and conditions them on a fire scenario that is a consequence rather than a causation. Therefore, fire scenarios should instead form part of the design outputs, uncovering a designer's capacity to positively affect the fire's potential nature and reduce its overall impact.

Based on the preceding, this paper aims to:

- Propose a hazard-centered and consequence-oriented approach for fire safety design that can explicitly compute fire scenarios as an analysis output. This paradigm shift enables simultaneously devising the structure and the resulting hazard scenario intensity, minimizing fire consequences and bounding them within acceptable thresholds.
- Use Monte Carlo sampling (MCS) to gain insights into the effect of selected input uncertainties on performance estimates.
- Demonstrate the proposed methodology's applicability and advantages through a simplified case study.

Consequence-Oriented Fire Intensity Optimization Approach

Terminology

Fire safety design methodologies should enable their integration into an iterative and holistic structural design process, representing the only strategy to deliver a truly optimized structure (e.g., Torero 2006; Maluk et al. 2017). This integration requires a uniform and harmonized terminology for risk analysis across multiple hazards. Thus, the following subsections define two terms that aid in developing the proposed consequence-oriented fire intensity optimization (CFO) approach: *consequence* and *fire modeling*. The methodology's name is then clarified.

Consequence

In a risk-based design framework, the hazard's *consequences* of interest may include repair costs, downtime, and casualty rates (among many others), quantified through probabilistic decision variables (e.g., Porter 2003). On the other hand, *damage analysis* refers to an intermediate step of the risk assessment process, which characterizes the physical impact of the hazard in a probabilistic fashion through fragility models.

A different terminology is found in the quantitative definition of risk by Kaplan and Garrick (1981), who denote the consequences of a hazard scenario as *damage*. Similarly, in the maximum allowable damage approach to fire safety by Cadena et al. (2022), the word *damage* refers to the consequence metric quantifying the following performance objectives: ensuring life safety, reducing direct and indirect economic losses, and designing a building that supports or eases firefighters' operations. From a risk-based design perspective, some metrics quantifying these objectives fall into the damage measures definition. For instance, structural integrity to guarantee resistance until burnout and firefighters' accessibility might be tested using damage measures for the structural components under investigation. However, other metrics (e.g., fatalities, property losses, downtime) would be categorized as decision variables. Thus, the general term *consequence* is suggested in this paper to denote both damage measures and decision variables.

Fire Modeling

The fire–structure coupling effect described previously renders fire safety assessments possible only if the combustion process and fire dynamics are characterized as a function of the surrounding. Based on these considerations, Torero (2013a) defined *fire modeling* as modeling the combustion process within the context of its environment. In the current study, this definition is used to emphasize the difference between fire and other hazards that can be characterized independently of the structure.

Khan et al. (2021) reviewed available fire modeling strategies ranging from standard temperature curves to complex computational fire dynamics models. In this regard, the effectiveness of the proposed design methodology in positively affecting the combustion process and fire dynamics relies on the selection of modeling strategies that capture the fire–structure coupling effect. More precisely, the simplicity of fire and heat transfer models defines the extent to which a designer can leverage the coupling to achieve a more optimized design solution.

Consequence-Oriented Fire Intensity Optimization

Fire prevention measures can lower the likelihood of fire occurrence. However, unplanned ignitions are inevitable over a structure's life cycle (e.g., Buchanan and Abu 2017). In this sense, a fire has an occurrence probability of 1 (Torero 2019), while the rare event is its evolution to an uncontrolled state. Such an evolution depends on the

structural context (fire–structure interaction) and the efficiency of the implemented fire safety strategy to control the fire. Hence, the design approach developed in this paper is *consequence-oriented*, i.e., it quantifies the fire risk in terms of maximum consequences (and their probabilistic distribution) for a certain fire scenario. The fire scenario maximizing consequences is calculated through numerical optimization and assumed to be characterized by a probability of 1.

Furthermore, the proposed methodology seeks to identify design variables that limit maximum consequences to an acceptable level, termed the maximum allowable consequence (MAC). This goal is achieved by optimizing the balance between increased structural member capacity and decreased fire intensity (*fire intensity optimization*). Stakeholders set the MAC in terms of consequence metrics of interest (e.g., casualties, economic losses, and downtime).

Methodology Description

The proposed CFO approach builds on the premise that every structure has a maximum consequence potential (MC), which depends on structural and hazard features. This assumption is analogous to that underlying the approach by Cadena et al. (2022). The MC describes the maximum consequence level that can derive from a fire event. Such a level should be lower than the MAC threshold.

Because of the complex interaction among the variables affecting the fire–structure coupling effect, the CFO approach uses optimization to calculate the MC. Next, the approach aims to identify design parameters defining a fire hazard scenario whose effects bind the MC below an acceptable threshold (the MAC).

The methodology is shown in Fig. 1 and consists of five steps. Step I defines the set of fire safety performance objectives, which typically include life safety, property protection, continuity of operations, and environmental protection (Hurley and Rosenbaum 2016). Following that, various end-users and decision-makers are called to select the acceptance threshold, i.e., the maximum level of consequence they are willing to accept (MAC). Such a threshold is generally set together with a fire design time, t_d, i.e., the time frame over which consequences should be calculated. Possible choices for t_d are (Buchanan and Abu 2017): (1) the time required for evacuation; (2) the time for firefighters to complete rescue activities and contain the fire; or (3) the time to burnout without intervention. It is observed that warranting structural integrity (or the nonexceedance of a selected limit state) for a specified t_d can also be taken as the consequence metric. Additionally, when considering different sources of uncertainty, an acceptable value of the probability of MC being greater than MAC can be selected. An initial design configuration $\mathbf{X}_1$, including structural and fire safety strategy features, is also selected in this step.

The following step (Step II) builds a consequence potential model $\mathrm{CP}(\mathbf{X}, \boldsymbol{\alpha})$ to quantify the potential of fire-induced consequences as a function of structural and fire safety strategy design variables and fire scenario variables, $\boldsymbol{\alpha}$. Such a model is obtained through numerical simulation of the structure's thermomechanical response to fire, which usually consists of three analysis steps: (1) fire modeling, entailing the heat release from the fire and the heat transfer to the structure; (2) thermal response; and (3) structural response.

In Step III, for a given realization of the design variables ($\mathbf{X} = \mathbf{X}'$), numerical optimization is adopted to compute MC. In this process, the fire scenario features maximizing consequences ($\boldsymbol{\alpha}_{\mathrm{MC}}$) are also obtained as a procedure output. Up to this stage, the procedure is deterministic. In this regard, several studies supported using deterministic methods for consequence assessment. Among others, Kirchsteiger (1999) discussed that, in safety science, deterministic analyses provide detailed insights into the consequence component of risk, independently of occurrence probabilities. Additionally, Paté-Cornell (1996) explained that deterministic analyses focused on consequences are adequate when the probabilistic distribution of critical variables is unknown. This is frequently the case in fire engineering. Deterministic analyses are also the basis for achieving an inherently safe design (Kletz and Amyotte 2010) and were embraced in the methodology by Cadena et al. (2022).

Nevertheless, understanding the effect of input uncertainties remains essential for safety assessment and decision-making. Indeed, when considering uncertainties (e.g., material and geometrical properties of structural components), the maximum consequence potential becomes a random variable $\overline{\mathrm{MC}}$, of which MC is a realization. Hence, Step IV implements Monte Carlo sampling to estimate the unknown distribution of $\overline{\mathrm{MC}}$ and calculate the probability $\Pr[\overline{\mathrm{MC}} > \mathrm{MAC}]$ that the MC is greater than the MAC. In this process, a designer is called to recognize input variables characterized by robust statistical data to capture their aleatory or epistemic uncertainty (Der Kiureghian and Ditlevsen 2009) and poorly characterized random variables. For the latter, conservative deterministic values are set. Importantly, the goal of Step IV is twofold:

- Capturing the effect of uncertainty propagation from the selected input variables; and
- Quantifying the solution's robustness to uncertainties, i.e., its limited sensitivity to input variations.

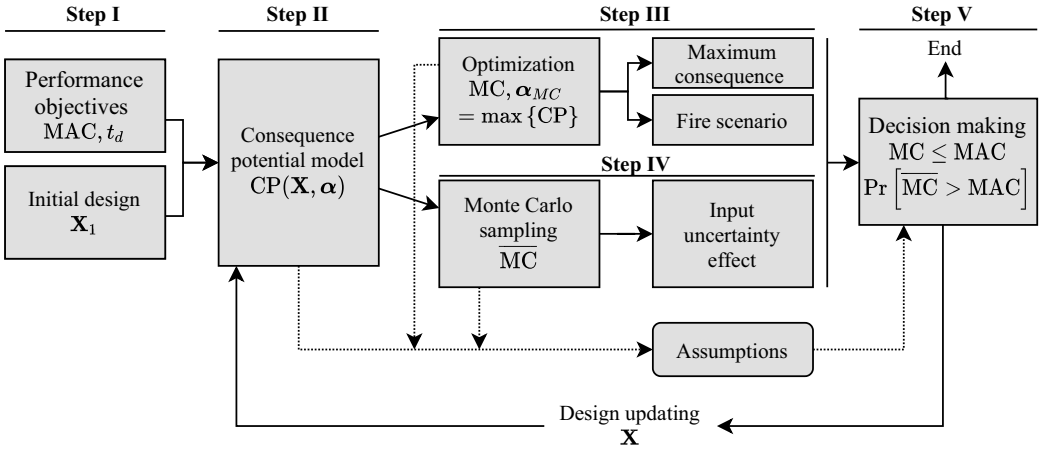

Fig. 1. Proposed CFO approach.

J. Struct. Eng., 2024, 150(4): 04024020

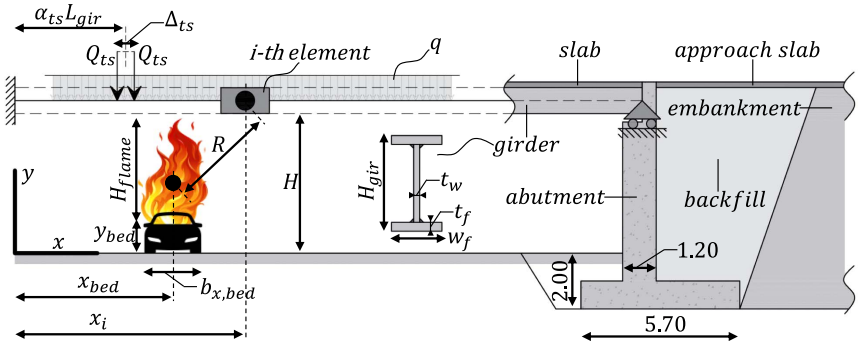

Fig. 2. Case study bridge: model, girder, and approach details.

Robustness can be quantified through dispersion statistics, such as the coefficient of variation (CoV) of $\overline{\text{MC}}$ (i.e., the ratio of the standard deviation to the mean).

The final step of the methodology (Step V) consists of decision-making. In this regard, a design configuration satisfying the condition $\text{MC} \leq \text{MAC}$ with an acceptably low $\Pr[\overline{\text{MC}} > \text{MAC}]$ complies with the performance objectives. Importantly, decision-making is also informed by examining the assumptions drawn throughout Steps II, III, and IV, which must be explicitly stated and tracked into the project documentation. Possible tools for assumption assessment include strength of knowledge and insensitivity verification (Cadena et al. 2020, 2022).

If a design for compliance is pursued, the fire performance of different design options can be assessed and compared through the CFO approach. Differently, in the design optimization case, a minimum for MC is searched while ensuring the compliance condition is verified. The minimum MC calculation aligns well with the recommendation of designing structures to obtain a minimum (fire) damage potential as an alternative to the use of design fires (Torero 2006).

In the next section, a single-span steel-girder bridge's fire safety design (for compliance) through the CFO approach is performed as an illustrative application. This case study is intentionally simplified to showcase the methodology's applicability, features, and possible outcomes. Among other simplifications and limitations, the fire–structure coupling effect is only exploited in its most straightforward realization, i.e., how the bridge clearance affects flame impingement, tilting, and lateral spread. The adopted model does not capture, for instance, the radiative heat feedback effects on the combustion process.

Illustrative Application

Case Study Description

As a proof of concept for the CFO approach, this section describes the fire safety design of a single-span bridge from the literature (Peris-Sayol et al. 2015b) exposed to vehicle-borne fires. This bridge, designed according to US standards, only serves as an initial configuration for assessment and update using the proposed methodology.

The structure is represented in Fig. 2, with the variable definition and values reported in Table 1. The deck is 5 m from the ground level (vertical clearance) and consists of five 21.34-m-long steel girders supporting a 0.20-m-thick concrete slab. Material properties are listed in Table 1. As specified in the reference (Peris-Sayol et al. 2015b), the girders are not rigidly connected to the slab. Thus, the steel-concrete composite action is neglected. The bridge approach details in Fig. 2 were estimated based on typical dimensions of cantilever abutments and rules of thumb for initial sizing (Parke and Hewson 2022; Clayton et al. 2014). Such information serves cost analysis in the following subsections. This study only considers the central girder of the bridge, which is analyzed in the x-y plane.

Table 1. Bridge structure properties

Variable type	Definition	Symbol	Value	Units
Geometric properties	Bridge girder length	L_{gir}	21.34	m
	Vertical clearance	H	5.00[a]	m
	Girder depth	H_{gir}	0.93[a]	m
	Flange width	w_f	0.424[a]	m
	Flange thickness	t_f	0.043[a]	m
	Web thickness	t_w	0.024[a]	m
Material properties	Steel elastic modulus	E	210.00	GPa
	Steel yielding stress	σ_y	250.00	MPa
	Steel density	ρ_{steel}	7,850.00	kg/m^3
	Concrete density	ρ_{concrete}	2,500.00	kg/m^3
Dead and live loads	Uniformly distributed load	Q	42.17	kN/m
	Double axle concentrated load	Q_{ts}	240.00	kN

[a]Initial design values: Design 1.

In the original reference, the girders are simply supported. However, Fig. 2 shows that a fixed end is assumed on the left-hand side. This choice aims to show the proposed approach's ability to determine fire scenarios as outputs (otherwise, the problem would be symmetric, and the most unfavorable condition would result from a fire at the midspan, where both the peak bending moment and the peak deflection are found). The fixed end might represent specific design details aimed at controlling the girders' deflection or could be a simplified analysis approach for a two-span continuous girder bridge.

Load Model 1 (Notional Lane 1) from EN 1991-2 (CEN 2003) is adopted to represent traffic loads. The model consists of a uniformly distributed load $q_1 = \alpha_{q1} \times 9$ kN/m^2 and two double-axle concentrated loads (tandem system) $Q_{ts} = \alpha_{Q1} \times 300$ kN. The α_{q1} and α_{Q1} are adjustment factors (here assumed equal to 0.8, which is the minimum value recommended by the Eurocode). The tandem system is located at $x_{ts} = \alpha_{ts} \times L_{\text{gir}}$ from the origin (Fig. 2). Here, L_{gir} is the girder length and α_{ts} is a general scaling factor that is to be determined to maximize consequences. Following these considerations, the load q in Fig. 2 consists of the sum of the girder's dead load, the superimposed dead load of the slab and bridge pavement, and q_1 described previously. It is acknowledged that using the Eurocode model to represent traffic loads may be acceptable for the illustrative application presented in this paper, where the bridge design serves only as an initial design configuration. However, it is

inconsistent with the location for which the structure was originally designed.

The fire scenario consists of a localized car fire situated at $x_{\text{bed}} = \alpha_{\text{bed}} \times L_{\text{gir}}$. The fuel bed has dimensions $b_{x,\text{bed}} \times b_{z,\text{bed}} = 1.5 \times 4.0$ m and is located at y_{bed} from the ground level. Details about the selected fire modeling approach are discussed in the subsections "Heat Release from the Fire" and "Heat Transfer." The fuel bed position, the fire model properties, and tandem system position maximizing consequences must be calculated.

Bridge design encompasses a wide range of design variables related to geometry, cross sections, and materials, and the number of variables can vary across different stages of the design process (from conceptual to detailed). For illustrative purposes, this study specifically focuses on the vertical clearance H, the girder depth H_{gir}, and the flange width w_f (see Fig. 2), which offer sufficient detail at the conceptual design stage. However, the proposed approach can accommodate a more extensive set of design variables. Changing H delays or avoids flame impingement at the deck level, reducing the heat flux to the girder (e.g., Peris-Sayol et al. 2015a). Differently, H_{gir} and w_f determine the section factor [ratio of heated perimeter to the cross-sectional area (Buchanan and Abu 2017)], to which the temperature rise in structural steel members is directly proportional. From a thermomechanical perspective, these two variables modify the girder moment of inertia—reducing deflections—and its bearing capacity. The properties listed in Table 1 are obtained from Peris-Sayol et al. (2015b) and represent the initial design configuration (addressed as Design 1).

The flange and the web thicknesses also play a significant role in determining the bridge's bearing capacity and stiffness. Furthermore, the flange's thickness might be critical to minimize girder and embankment height while fulfilling structural requirements. In this study, the flange and web thicknesses are defined as a function of H_{gir} and w_f to maintain the same thickness ratio as Design 1. In this way, the section classification according to EN 1993-1-1 (CEN 2005a) remains Class 1 (plastic cross section) in any design configuration.

The thickness of a fire protection layer could also be considered a design variable. Nevertheless, bridge girders are typically not protected (Payá-Zaforteza and Garlock 2012; Kodur et al. 2013). In addition, Hu et al. (2021) highlighted the need for research to improve the resistance of bridges without fire protection. Therefore, fire protection is not considered in this paper. The design variables for the general bridge configuration k are defined as a fraction of those in Design 1. Thus, the design problem consists in determining the components of the following vector to comply with the performance objectives:

$$\mathbf{X}_k = [X_{H,k}, X_{H\text{gir},k}, X_{wf,k}] \tag{1}$$

In this equation, $X_{H,k} = H_k/H_1$; $X_{H\text{gir},k} = H_{\text{gir},k}/H_{\text{gir},1}$; and $X_{wf,k} = w_{f,k}/w_{f,1}$.

Performance Objectives

Several vehicle fires were considered in the literature, including car, heavy goods vehicle, bus, and truck fires. Nevertheless, for illustrative purposes, only car fires are considered in this paper. Thus, the performance objectives are set in terms of time for the bridge to reach unsatisfactory conditions (t_u) when subject to a car fire. Here, *unsatisfactory conditions* refer to the bridge collapse, which is assumed to occur when the studied girder collapses. As t_u decreases, the available time for the fire service to control the fire also decreases. Hence, more severe consequences are associated with lower values of t_u. For illustrative purposes only, it is assumed that stakeholders require the bridge to resist any car fire accident for $t_{u,\text{MAC}} = 20$ min without collapsing. A fire exposure of the same duration was considered in previous studies (e.g., Hu et al. 2018).

A design solution k is acceptable if $t_{u,\text{MC},k} \geq t_{u,\text{MAC}}$. The effect of uncertainties (i.e., $\Pr_{\text{MC>MAC}} = \Pr[\bar{t}_{u,\text{MC},k} < t_{u,\text{MAC}}]$), the assumptions drawn to build the consequence model, and the total cost are also accounted for in the decision-making process. In the current example, $\Pr_{\text{MC>MAC}}$ is also applied to compare design solutions through the total bridge cost (Moses 1977)

$$C_T = C_I + \Pr_{\text{MC>MAC}} \times C_F \tag{2}$$

In this equation, C_T = total cost; C_I = initial cost; and C_F = expected failure cost, obtained as the sum of direct ($C_{F,\text{dir}}$) and indirect ($C_{F,\text{ind}}$) costs caused by the bridge failure. Indirect costs include the economic losses associated with the road's closure (due to inspection and repairs), such as traffic delays, detours, and business interruption. The consequence metric C_T represents a simplified version of the life-cycle cost. Indeed, the latter includes other cost items, such as the inspection and maintenance cost (e.g., Alipour et al. 2011). For this calculation, the following simplifying assumptions are drawn (see the Appendix for further discussion):

- C_I and $C_{F,\text{dir}}$ only account for the construction material costs.
- The unit material costs from the Washington State DOT (2022) and unit bid analysis history data (Washington State DOT 2023) are used (Table 2).
- $C_{F,\text{dir}}$ equals the superstructure material cost.
- Quantifying $C_{F,\text{ind}}$ requires a comprehensive analysis of the bridge's infrastructural network and the surrounding region, which is beyond the scope of this paper. Hence, for simplicity, an estimated indirect loss of \$8.55 million/day, as calculated by Limongelli et al. (2018), is considered. Furthermore, restoring the bridge's functionality is assumed to take 30 days. These values are comparable with the fire-induced collapse consequences of the MacArthur Maze bridge (Garlock et al. 2012), which was reopened 26 days after the incident and caused about \$6 million/day of losses.
- A reinforcement ratio of 2% is considered for the slab and the abutment.

The nondimensional costs are defined by taking ratios to the reference initial cost for Design 1 (i.e., $c_I = C_I/C_{I,1}$, $c_F = C_F/C_{I,1}$, and $c_T = C_T/C_{I,1}$). It is noted that design solutions could also be compared in terms of consequence metrics that address sustainability targets (e.g., the embodied carbon of the structure).

Table 2. Unit material costs

Item	Unit cost
Approach slab[a]	\$299/m^2
Bearing	\$125 each
Structural carbon steel (girder)	\$5/kg
Substructure concrete (Class 4000)	\$654/m^3
Superstructure concrete (Class 5000)	\$1,373/m^3
Steel reinforcement bar	\$3/kg
Traffic barrier	\$459/m
Gravel backfill[b]	\$105/m^3

[a]Assumed dimensions: 13×8 m.
[b]Based on unit bid analysis history data from the Washington State DOT (2023).

Consequence Potential Model

Because the time to reach unsatisfactory conditions is adopted as the performance metric, the consequence potential model is $t_u(\mathbf{X}, \boldsymbol{\alpha})$. Such a model can be obtained through the three steps listed in the

section "Methodology Description," for which further details are provided in the following subsections.

Heat Release from the Fire

The car fire is modeled through a bilinear HRR function representing the time history $\mathrm{HRR}(t)$ of the amount of energy released by the fire. The HRR starts at the time of ignition and grows linearly up to a peak HRR, $\mathrm{hrr}_{\max}$, which is reached at the time $t_{\max}$. Then the curve remains constant until burnout (t_{bo}). The total energy released by the burning vehicle, named ER, is obtained by integrating $\mathrm{HRR}(t)$ over time. For a fixed ER value, different combinations of $\mathrm{hrr}_{\max}$ and $t_{\max}$ result in different HRR time histories, spanning from a short-hot to a long-cool fire. In general, the available mass of fuel defines ER; $t_{\max}$ depends on the flame spread rate, which in turn is a function of the thermal conductivity of the burning material; finally, $\mathrm{hrr}_{\max}$ depends on the burning area, burning rate, and heat of combustion of the fuel.

Table 3 summarizes the fire modeling parameter definition and values. The peak heat release rate, the time to reach it, and the total energy released are based on experimental data from the literature (Mohd Tohir and Spearpoint 2013). Fig. 3 shows these parameters' statistical distribution. For fire safety design purposes, a maximum ER value should be set by stakeholders. Here, for illustration, a conservative value ER = 7 MJ is assumed.

On the other hand, conservative values for $\mathrm{hrr}_{\max}$, $t_{\max}$, and their combination cannot be set a priori. Indeed, a short-hot fire might create the most demanding conditions (i.e., faster average temperature rise and material degradation) for a girder made of thin steel plates. Conversely, with equal ER, a long-cool fire might represent the most severe condition for a girder with a low section factor.

Table 3. Fire modeling properties

Variable definition	Symbol	Value	Units
Time history of the heat release rate	$\mathrm{HRR}(t)$	Time-varying	$\mathrm{kW/m^2}$
Peak heat release rate	$\mathrm{hrr}_{\max}$	[2, 8]	$\mathrm{MW/m^2}$
Time to the peak HRR	$t_{\max}$	[6, 14]	min
Time to burnout	t_{bo}	$t_{\max}/2 + \mathrm{ER}/\mathrm{hrr}_{\max}$	min
Total energy released	ER	7.0	GJ
Fuel bed size (x-axis)	$b_{x,\mathrm{bed}}$	1.5	m
Fuel bed size (z-axis)	$b_{z,\mathrm{bed}}$	4.0	m
(Average) flame height	H_{flame}	Time varying	m
Fuel bed location (x-axis)	x_{bed}	$[b_{x,\mathrm{bed}}/2, L_{\mathrm{gir}} - b_{x,\mathrm{bed}}/2]$	m
Fuel bed location (y-axis)	y_{bed}	1.0	m

Lamont et al. (2004) discussed that in composite sections, a short-hot fire generally leads to a higher peak temperature and a more pronounced thermal gradient, resulting in bowing. Instead, a long-cool fire produces a more uniform temperature distribution and greater thermal expansion. In both cases, if the thermal strains are restrained, mechanical strains (and consequently stresses) arise (Sanad et al. 2000a). The combined effect of thermal expansion, bowing, and cross-sectional characteristics can result in a wide range of deflected shapes and axial forces, ranging from restrained expansion-dominated to gradient-dominated problems (Sanad et al. 2000b). Payá-Zaforteza and Garlock (2012) and Alos-Moya et al. (2014) discussed the impact of longitudinal restraints and thermal gradients on steel-girder bridges. In particular, thermal gradients might affect the structural response even if the concrete slab is not structurally connected to the girders (as in the current example). More details are provided in the Appendix. The simplifying assumptions drawn in the current case study (see subsequent discussion and the Appendix) render it representative of an intermediate case of balanced thermal expansion and thermal gradients (Sanad et al. 2000b).

In the essence of the CFO approach, $\mathrm{hrr}_{\max}$ and $t_{\max}$ maximizing consequences must be calculated. Such an analysis is performed through numerical optimization (Step III in Fig. 1) and requires selecting ranges of variation (or boundary conditions) for the two parameters. Representative values from NFPA 502 (NFPA 2020) are presented in Fig. 3 and are considered as the reference case ($\mathrm{hrr}_{\max,\mathrm{ref}} = 5$ MW, $t_{\max,\mathrm{ref}} = 10$ min). Then variation ranges of $\pm 60\%$ and $\pm 40\%$ with respect to the reference case are chosen for $\mathrm{hrr}_{\max}$ and $t_{\max}$, respectively. A more limited variability for $t_{\max}$ is chosen because a slowly growing fire—with $t_{\max}$ close to $t_{u,\mathrm{MAC}}$—would allow enough time to be detected and controlled. The two parameters $\mathrm{hrr}_{\max} = \alpha_{\mathrm{hrrmax}} \times \mathrm{hrr}_{\max,\mathrm{ref}}$ and $t_{\max} = \alpha_{t\max} \times t_{\max,\mathrm{ref}}$ can then describe a general HRR curve. Finally, a vector of fire scenario features is defined as $\boldsymbol{\alpha} = [\alpha_{\mathrm{bed}}, \alpha_{\mathrm{hrrmax}}, \alpha_{t\max}, \alpha_{ts}]$. These scaling factors refer to the fuel bed location, peak HRR, time to peak HRR, and tandem system location, respectively. Fig. 4 shows the selected HRR curve range and compares it with the experimental results from Mohd Tohir and Spearpoint (2013).

Heat Transfer

This section describes the calculation of heat flux $\dot{q}''_{\mathrm{fire}}$ from the fire to the bridge girder. The girder is divided into elements of 0.5 m in length (Fig. 2), and it is assumed that the heat flux to a given element is constant for a given time step. The element length was chosen based on a sensitivity study on the accuracy of the t_u prediction. The proposed heat transfer calculation procedure is summarized in

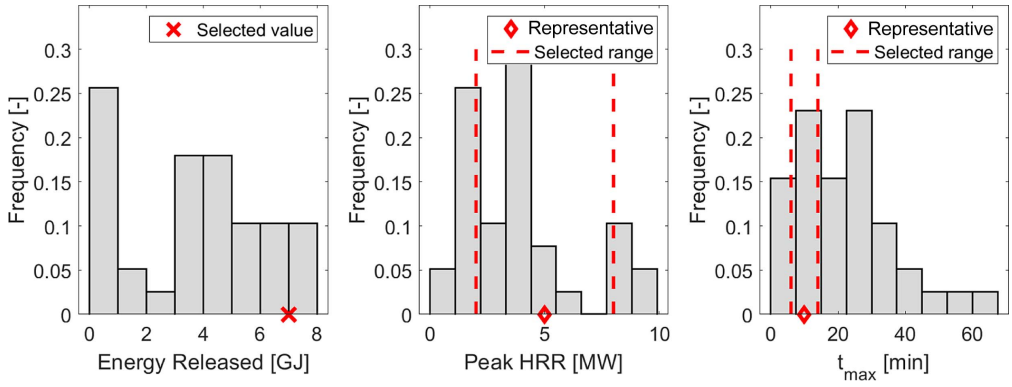

Fig. 3. Distributions of the total energy released, peak heat release rate and time to peak heat release rate. (Data from Mohd Tohir and Spearpoint 2013; NFPA 502 2020.)

J. Struct. Eng., 2024, 150(4): 04024020

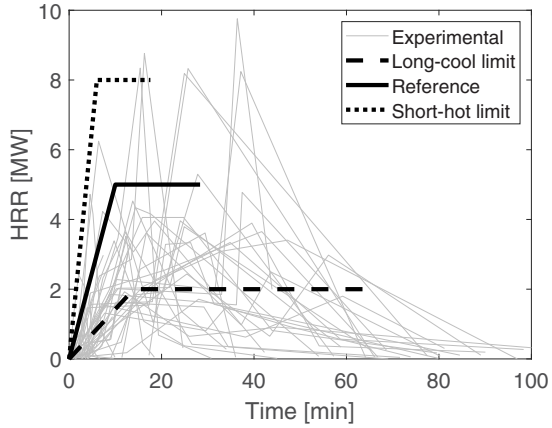

Fig. 4. Assumed HRR curve limits and comparison with envelopes of experimental data. (Data from Mohd Tohir and Spearpoint 2013.)

Table 4 and combines several radiative and convective heat transfer models from localized fires. The mean flame height H_{flame} is defined as the distance above the fuel bed at which the flame intermittency reduces to 0.5 (Zukoski et al. 1985) and is computed according to Heskestad (2016)

$$H_{\text{flame}} = -1.02D_{eq} + 0.235[\text{HRR}(t)]^{2/5} \tag{3}$$

where t = time; and D_{eq} = equivalent diameter, which, for noncircular fire sources, can be obtained as $D_{eq} = \sqrt{4b_{x,\text{bed}}b_{z,\text{bed}}/\pi}$. In this study, the minimum between this value and the minimum vehicle size is conservatively taken as D_{eq}. The value of H_{flame} is then compared to the bridge's clearance, distinguishing the two cases of flames not impinging (Case 1) or impinging (Case 2) on the bridge deck. In Case 1, each girder element is classified based on its x-axis location x_i falling within ($|x_i - x_{\text{bed}}| \le D_{eq}/2$) or outside ($|x_i - x_{\text{bed}}| > D_{eq}/2$) the fuel bed boundaries. The plume temperature T_p at the height of the deck is then computed through Heskestad's correlation for centerline excess temperature (Heskestad 2016) and used to calculate the heat flux to elements within the bed boundaries

$$\dot{q}''_{\text{plume}} = h_c(T_p - T_{\text{ele}}) + \varepsilon\sigma(T_p^4 - T_{\text{ele}}^4) \tag{4}$$

where T_{ele} = temperature of the considered girder element; $\varepsilon = 1$ is the emissivity of the gas; $\sigma = 5.67 \times 10^{-8}$ W/m^{2}K^4 is the Stefan-Boltzmann constant; and h_c = convective heat transfer coefficient, which depends on the fluid properties, flow parameters, and surface geometry. This coefficient typically spans in the range 5 − 50 W/m^{2}K (e.g., Drysdale 2011; Welty et al. 2020) and is here assumed equal to 25 W/m^{2}K (e.g., Jowsey 2006). Additionally, assuming that a small optical thickness characterizes the smoke, the radiative heat flux from the flame $\dot{q}''_{\text{flame}}$ is summed to $\dot{q}''_{\text{plume}}$ to determine $\dot{q}''_{\text{fire}}$. Flame radiation is estimated through the point-source model (Beyler 2016). The point source is located at the center of the flame volume. Only the radiative heat flux from flame is instead considered for girder elements outside the fuel bed boundaries.

In Case 2, the flames impinge on the bridge deck and their front spread in the longitudinal bridge direction (x-axis). In such a situation, Heskestad and Hamada (1993) observed that the mean horizontal flame length L_{flame} is approximately equal to the difference between the free flame height and the height of the obstructing surface. A constant value of heat flux $\dot{q}''_{\text{flame}} = 85$ kW/m^2 is assigned to girder elements whose center locates within a distance L_{flame} from the center of the fuel bed. This value is representative of measured heat fluxes to objects immersed in flames (Lattimer 2016). Furthermore, it represents a conservative assumption with respect to the 20 − 70 kW/m^2 range suggested by Shaw et al. (2016) for tunnel fires. Only radiative heat fluxes are instead considered for girder elements that are not in contact with the flames.

Thermal Response

The thermal response of each girder element is calculated through a lumped thermal mass approach [e.g., Quiel et al. 2015; Zhu et al. 2020; EN 1993-1-2 (CEN 2005b)]. This approach assumes a constant temperature distribution across the section (lumped capacitance), which is acceptable for steel girders. At each iteration time t_j, the temperature increase $\Delta T_{i,j}$ in the ith girder element is calculated through the energy balance equation (the index j is not shown for simplicity):

$$\Delta T_i = \frac{dt}{\rho_{\text{steel}} V_i c_p(T)} \times (\dot{Q}_{\text{fire},i} - \dot{Q}_{\text{out},i} + \dot{Q}_{i-1,i} + \dot{Q}_{i,i+1}) \tag{5}$$

In this equation, dt = time step; ρ_{steel} = density of steel, defined in Table 1; V_i = ith girder element volume; $c_p(T)$ = temperature-dependent specific heat of steel [EN 1993-1-2 (CEN 2005b)]; $\dot{Q}_{\text{fire},i}$ = heat transferred from the fire, calculated as $\dot{q}''_{\text{fire}}A_{\text{exp}}$; A_{exp} = exposed surface of the girder; $\dot{Q}_{\text{out},i}$ = heat loss to the ambient from the unexposed side of the girder; and $\dot{Q}_{i-1,i}$ and $\dot{Q}_{i,i+1}$ = conductive heat transfer terms from the element $i-1$ to i and from the element i to $i+1$, respectively. The latter two terms are calculated considering a temperature-dependent thermal conductivity coefficient [EN 1993-1-2 (CEN 2005b)]. The exposed surface A_{exp} is taken as the total surface of the girder net of the upper flange surface in contact with the concrete slab, whereas the ambient temperature is assumed as 20°C. Other studies that used the lumped capacitance approach (e.g., Quiel et al. 2015) recommended a maximum time step of 1 min. In this paper, to guarantee a more accurate prediction of t_u, a time step of 2 s is selected. The calculations described up to this point are implemented in the MATLAB software and provide input files of temperature time histories in each girder element. These time histories are used for finite-element analysis as discussed in the next subsection.

Table 4. Heat flux calculation methodology

Case	Girder region	Heat flux model
Case 1: No flame impingement $y_{\text{bed}} + H_{\text{flame}} \le H + H_{\text{gir}}$	$\lvert x_i - x_{\text{bed}}\rvert \le D_{eq}/2$	Convective and radiative heat transfer from the plume: Heskestad's correlation for centerline excess temperature (Heskestad 2016). Radiative heat transfer from the flames: point-source model (Beyler 2016).
	$\lvert x_i - x_{\text{bed}}\rvert > D_{eq}/2$	Radiative heat transfer from the flames: point-source model (Beyler 2016).
Case 2: Flame impingement $y_{\text{bed}} + H_{\text{flame}} > H + H_{\text{gir}}$	$\lvert x_i - x_{\text{bed}}\rvert \le L_{\text{flame}}$	Constant heat flux to object immersed in flames $\dot{q}''_{\text{flame}}$ (Lattimer 2016)
	$\lvert x_i - x_{\text{bed}}\rvert > L_{\text{flame}}$	Radiative heat transfer from the flames: point-source model (Beyler 2016).

Table 5. Considered failure criteria for the girder

Failure condition	Assessment criterion
Runaway behavior of girder deflection (Payá-Zaforteza and Garlock 2012; Hu et al. 2018, 2021)	Vertical deflection rate of any girder node exceeding 0.5 m/min
Reversal of horizontal displacement at the free end support (Payá-Zaforteza and Garlock 2012; Hu et al. 2018, 2021)	Horizontal displacement rate of any girder node lower than 0 m/min
Excessive vertical deflection [BS 476-20 (BSI 1987)]	Vertical deflection of any girder node exceeding $L_{gir}/20$

Structural Response

The mechanical response of the bridge is estimated through the OpenSees for Fire software (Jiang et al. 2015). Specifically, the girder is modeled using displacement-based elements with thermomechanical fiber sections. Each fiber is assigned the uniaxial material *Steeel01Thermal* (Jiang et al. 2015), which includes the temperature-dependent properties from EN 1993-1-2 (CEN 2005b). The displacement history of each girder node is monitored during the thermomechanical analysis, which starts from the deformed configuration induced by dead and traffic loads. Finite-element simulations use the same time step as the thermal analysis and run until t_{bo}, unless the bridge collapses before the fuel burnout.

Failure criteria should be defined to calculate t_u. This paper only considers global failure, assumed to occur when any of the conditions listed in Table 5 verifies. The vertical and horizontal displacement rate limits are based on sensitivity studies by the authors, which exhibited an agreement in the ±5% range between the t_u obtained through the two criteria. These results refer to the structural configuration considered in this paper, and further analyses are required to generalize their application. If the bridge resists until burnout without collapsing, an infinite time to untenable conditions ($t_u \to \infty$) is considered for that design configuration.

The following subsections present the results obtained by applying the CFO approach to the previously outlined case study. Because several simplifying assumptions were drawn to build the consequence potential model, the Appendix comprehensively discusses their limitations. This discussion emphasizes that the case study serves purely illustrative purposes and does not intend to provide definite results.

Maximum Consequence Potential and Design Updating

For the kth design configuration $\mathbf{X}_k$, the minimum time to unsatisfactory conditions ($t_{u,\mathrm{MC},k}$) and the corresponding fire scenario vector $\boldsymbol{\alpha}_{\mathrm{MC},k}$ are obtained by numerical optimization (Step III in Fig. 1) using the MATLAB software. More precisely, the MC is obtained by fixing $\mathbf{X}_k = \mathbf{X}'_k$ and solving the following optimization problem:

$$t_{u,\mathrm{MC},k}, \boldsymbol{\alpha}_{\mathrm{MC},k} = \min\{t_u(\boldsymbol{\alpha}, \mathbf{X}'_k)\}, \quad \text{subject to } \boldsymbol{\alpha}_{LB} \le \boldsymbol{\alpha} \le \boldsymbol{\alpha}_{UB} \tag{6}$$

In this equation, $\boldsymbol{\alpha}_{LB}$ and $\boldsymbol{\alpha}_{UB}$ represent boundary conditions and are defined in Table 6. First, the fuel bed location limits are found by assuming its proximity to the abutments. Second, the limits for the HRR curve variable scaling factors $\alpha_{t\mathrm{max}}$ and α_{hrrmax} are calculated by dividing the range limits defined in the section "Heat Release from the Fire" by their reference values. Finally, the bounds for the tandem system position are set to maintain the two axial loads of the tandem system on the girder.

For the initial design configuration (Design 1, $\mathbf{X}_1 = [1, 1, 1]$) the MC results $t_{u,\mathrm{MC},1} = 11.47$ min and derives from a fire scenario $\boldsymbol{\alpha}_{\mathrm{MC},1} = [0.654, 1.580, 0.608, 0.631]$. Because the time to untenable conditions is significantly lower than the allowable threshold $t_{u,\mathrm{MAC}} = 20$ min, design updating as per Fig. 1 is required.

Table 6. Boundary conditions for the fire scenario

Parameter	Fuel bed location	Peak HRR	Time to peak HRR	Tandem system location
Scaling factor	α_{bed} [-]	α_{hrrmax} [-]	$\alpha_{t\mathrm{max}}$ [-]	α_{ts} [-]
Lower bound (LB)	0.035	0.4	0.6	0.028
Upper bound (UP)	0.965	1.6	1.4	0.972

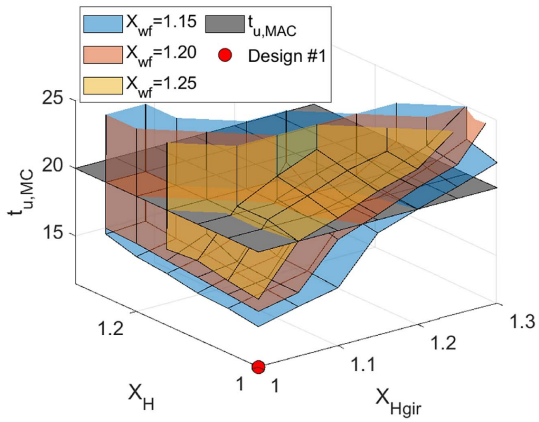

Fig. 5. Sensitivity study on the effect of design variables on maximum consequence potential.

To that end, a sensitivity study on the effect of the three selected design variables on the MC is performed through full factorial design, varying the design variable's scaling factors in the [1.00-1.30] range. Representative results are shown in Fig. 5, which plots $t_{u,\mathrm{MC}}$ versus X_H and $X_{H\mathrm{gir}}$. The three surfaces correspond to $X_{wf} = 1.05, 1.15$, and 1.25, whereas the marker shows Design 1. In this figure, the intersection between the plane $t_{u,\mathrm{MC}} = t_{u,\mathrm{MAC}}$ and a surface divides compliant (with performance objectives) and noncompliant design configurations. Based on the sensitivity study, the four design configurations in Table 7 are selected (Designs 2–5). Section factors, moments of inertia, and consequence metrics are also reported. Further reasoning for the chosen designs is provided in the following. Design 2 yields a $t_{u,\mathrm{MC},1} = 19.33$ min close to—but lower than—$t_{u,\mathrm{MAC}}$ and is selected to explore its possible benefits when considering uncertainties. Designs 3 and 4 consist of significantly different design variables but provide a similar $t_{u,\mathrm{MC}}$, close to the MAC threshold. Thus, they are selected to discuss the feature of cost-effective solutions. Finally, Design 5 is characterized by the highest $t_{u,\mathrm{MC}}$ and is therefore expected to provide the most significant margin of safety with respect to $t_{u,\mathrm{MAC}}$.

Fire scenario variables resulting in the maximum consequences (Table 7) are represented in Fig. 6. Specifically, Fig. 6(a) compares the fuel bed and tandem system location. Two horizontal lines of the same color represent the girder's top and bottom flanges, whereas the vertical, dashed lines ease the location comparison.

Table 7. Design configuration comparison

Parameter	Symbol	Units	Design 1	Design 2	Design 3	Design 4	Design 5
Design variables	X_H	—	1.00	1.00	1.05	1.00	1.10
	$X_{H\text{gir}}$	—	1.00	1.10	1.20	1.10	1.25
	X_{wf}	—	1.00	1.20	1.15	1.25	1.15
Section factor	H_p/A	m^{-1}	54.64	46.07	47.14	44.40	46.73
Moment of inertia	I_{zz}	$\times 10^{-3}$ m^4	8.33	14.03	16.16	14.99	17.85
Fire scenario	$\alpha_{\text{bed,MC}}$	—	0.654	0.734	0.734	0.782	0.750
	$\alpha_{\text{hrrmax,MC}}$	—	1.580	1.343	1.272	1.275	1.073
	$\alpha_{t\text{max,MC}}$	—	0.608	0.611	0.612	0.613	0.618
	$\alpha_{ts,\text{MC}}$	—	0.631	0.721	0.696	0.743	0.685
Consequence metrics	$t_{u,MC}$	min	11.47	19.33	20.23	20.93	22.17
	$\Pr[\tilde{t}_{u,\text{MC}} < t_{u,\text{MAC}}]$	—	1.000	0.216	0.026	3.10×10^{-3}	1.60×10^{-5}
	$\text{Cov}(\tilde{t}_{u,\text{MC}}\|\text{collapse})$	—	0.040	0.038	0.021	0.019	0.036
	c_I	—	1.000	1.095	1.120	1.115	1.151
	c_T	—	277.171	60.867	8.336	1.972	1.155

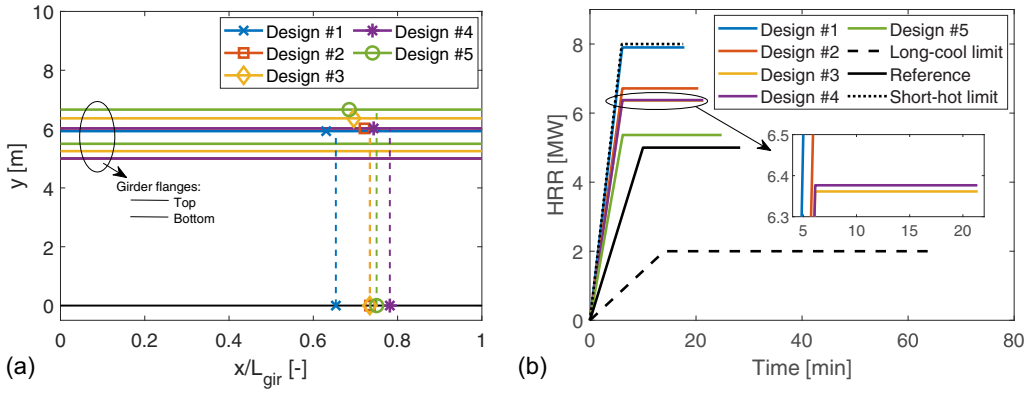

Fig. 6. Comparison of fire scenarios yielding maximum consequences: (a) fuel bed and tandem system location; and (b) HRR curves.

Fig. 6(b) shows the HRR time histories required to collapse the girder in the shortest time. The following observations are drawn:

- The MC fuel bed and tandem system locations [Fig. 6(a)] vary in the 13.95–16.68 m and 13.45–15.86 m ranges, respectively. Notably, the two points are generally not aligned, with their distance spanning from 0.08 m for Design 2 to 1.39 m for Design 5. When compared with the fuel bed dimension ($b_{x,\text{bed}} = 1.5$ m) and the point load distance in the tandem system ($\Delta_{ts} = 1.2$ m), the position difference is significant. It is also observed that neither x_{bed} nor x_{ts} correspond to the points of maximum bending and maximum deflection for a fixed-roller beam subject to uniformly distributed load ($x = 0.625L_{\text{gir}}$ and $x = 0.579L_{\text{gir}}$, respectively). These two points might be taken as intuitive, preliminary design assumptions in a design framework that starts from defining a hazard scenario.
- All the HRR time histories in Fig. 6(b) lay between the reference and short hot limit, stating that a rapidly growing fire is more damaging than a long-cool one (for the considered structure). Nevertheless, the curves are noticeably different from each other. Therefore, maximum consequences do not originate from the shortest, hottest fire but are structure specific, and their selection without considering this dependence undermines achieving the performance objectives. Indeed, a design approach that starts from defining fire scenarios would only analyze consequences induced by reference or limit HRR curves or implement sensitivity analysis. In both cases, the identification of scenario properties maximizing consequences is trivial.
- Table 7 shows that the five design configurations entail different section factors and moment of inertia combinations. Designs 2–5 exhibit section factors lower than Design 1. Consistently, Fig. 6(b) shows that a more prolonged fire exposure is required to heat the section to a level that steel properties deteriorate and cause collapse. Because the energy released is fixed, a longer fire exposure can only result from a lower peak HRR.
- The section factor alone is not sufficient to interpret and determine the fire scenario maximizing consequences. For instance, Designs 4 and 5 have section factors of 44.40 and 46.73 m^{-1}, respectively. Thus, Design 4 heats slower. However, a higher moment of inertia endows Design 5 with a longer time to untenable conditions. Hence, the fire scenario maximizing consequences can only be identified in the context of its environment, i.e., only considering the thermomechanical response of the system.

These considerations show that fire scenarios maximizing consequences vary significantly for diverse design configurations. Furthermore, the conditions that maximize fire impacts can neither be determined independently of structural properties nor assumed as input variables for fire safety design. Instead, they should be obtained as analysis outputs together with design variables. It is also essential to note that altering the design variables modifies the features of the fire scenario. Hence, an appropriate selection of the structural configuration positively affects the physics of the fire phenomenon, unveiling the possibility of a simultaneous design of the fire and the structure.

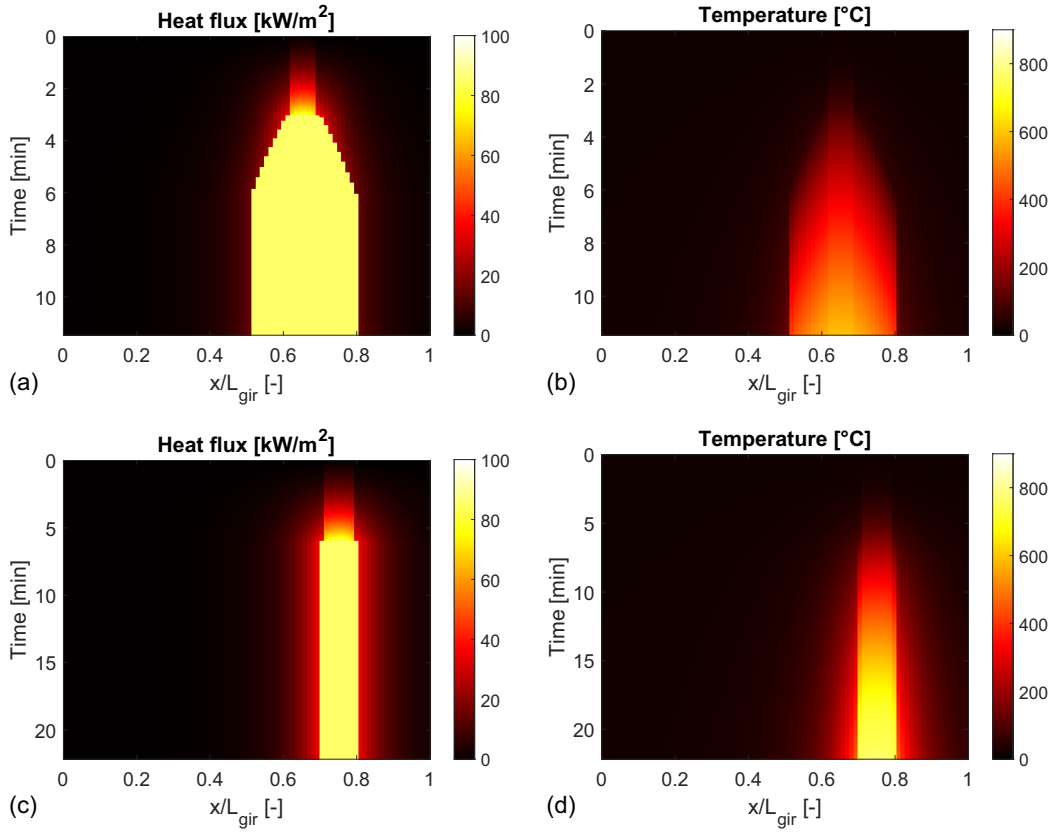

Fig. 7. Time history of the heat flux from the fire and girder temperature until untenable conditions: (a and b) Design 1, $t_{u,\mathrm{MC},1} = 11.47$ min; and (c and d) Design 5, $t_{u,\mathrm{MC},5} = 22.17$ min.

For instance, Fig. 7 compares the heat flux and temperature time histories for Designs 1 and 5. The increased clearance of Design 5 [combined with the HRR features of Fig. 6(b)] delays the time to impingement (from 5.9 to 6.7 min). Moreover, it significantly reduces the lateral flame spread (from 6.47 to 2.5 m, −61.36%). Consequently, the girder's temperature increase is retarded and restricted to a more limited part. Combining these effects with the increased inertia and reduced section factor, Design 5 collapses after 20.23 min of fire exposure, which complies with the MAC threshold. This result is achieved regardless of the higher peak temperature (876°C versus 593°C, +47.72%) that Design 5 reached.

Uncertainty Analysis

A further objective of the CFO approach is assessing input uncertainties' effect on the estimated MC (Step IV in Fig. 1). Plain MCS (Beck and Zuev 2015) is adopted for this aim. This study aims to assess the effect of the steel material properties uncertainty on $t_{u,\mathrm{MC}}$. The considered random variables (and their probability models) are given in Table 8 and were obtained from the work of Devaney (2015).

For each design configuration, MCS provides estimates for the random variable $\bar{t}_{u,\mathrm{MC}}$, its CoV, and the probability $\mathrm{Pr}_{\mathrm{MC>MAC}}$. The required sample size was calculated based on the target CoV for $\mathrm{Pr}_{\mathrm{MC>MAC}}$, aiming to estimate probabilities as low as 0.0001 with a CoV lower than 10%. The results are presented in Table 7.

Table 8. Considered random variables

Variable	Distribution	Mean	CoV	Units
Yielding stress	Lognormal	281	0.07	MPa
Elastic modulus	Lognormal	210	0.03	GPa
Density	Normal	7,850	0.01	kg/m^3

Source: Data from Devaney (2015).

The probability that the time to unsatisfactory conditions is lower than the minimum acceptable limit ranges between 1.60×10^{-5} for Design 5 and 0.216 for Design 2. For Design 1, the MAC threshold locates in the tail of $\bar{t}_{u,\mathrm{MC},1}$ (about 15 standard deviations from the mean) and is characterized by a negligible frequency. Thus, for this case, $\mathrm{Pr}_{\mathrm{MC>MAC},1}$ was taken as 1.

The CoV values in Table 7 reveal that Design 4 encompasses the highest robustness to uncertainties $[\mathrm{CoV}(\bar{t}_{u,\mathrm{MC},4}) = 0.019)]$. Differently, the largest dispersion is found for Design 2, with $\mathrm{CoV}(\bar{t}_{u,\mathrm{MC},2}) = 0.038$.

Decision-Making

Decision-making is based on the analysis of the consequence metrics in Table 7, which are plotted in Fig. 8 to ease the comparison. If safety is prioritized, stakeholders can opt for Design 5 (largest moment of inertia and clearance among the updated designs), which entails a failure probability of 1.60×10^{-5} and requires an initial cost 15.1% larger than Design 1. In this case, the low probability of failure copes with the lower robustness to uncertainty with respect to other configurations $[\mathrm{CoV}(\bar{t}_{u,\mathrm{MC},5} = 0.036)]$. On the other hand, if the initial cost is the guiding principle and a failure probability equal to 0.216 is tolerable, the choice falls on Design 2 (smallest moment of inertia among the updated designs and no increase in bridge clearance). The acceptability of such a significant failure probability might be motivated by the short time required to evacuate the considered bridge in the case of a fire so that collapse does not threaten life safety. However, Design 2 exhibits a considerable

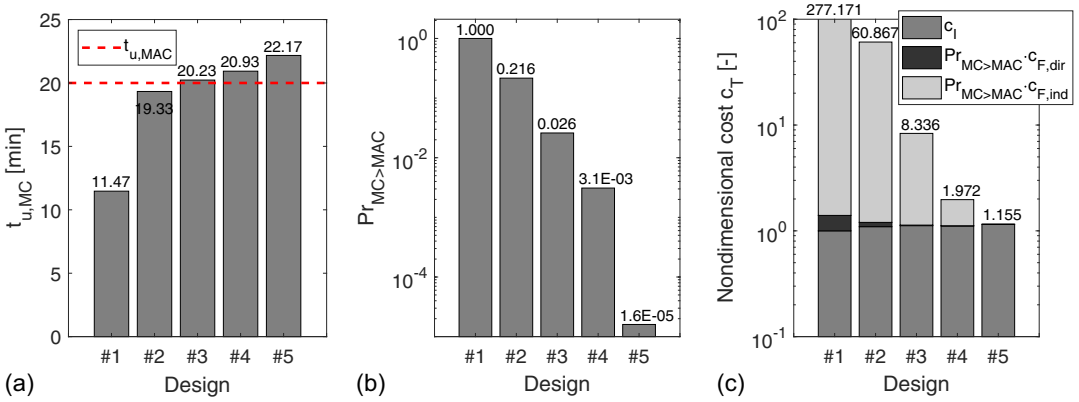

Fig. 8. Performance metric comparison.

total nondimensional cost ($c_{T,2} = 60.867$) due to the large failure probability that amplifies indirect losses. The remaining two design options gain interest when the total cost is considered. Despite the similar $t_{u,\mathrm{MC}}$ values, Design 3 (second largest moment of inertia among the updated designs and 5% increased clearance) and Design 4 (smallest section factor among the updated designs and no increase in bridge clearance) show failure probabilities differing by one order of magnitude (2.6×10^{-2} versus 3.1×10^{-3}). As a result, the total cost of Design 3 is about four times that of Design 4. This observation highlights the importance of investigating input uncertainty and how design choices propagate it. Consistent with the lower failure probability, Design 4 yields a total cost $c_{T,4} = 1.972$ upfront an initial cost increase of 11.5%. A further argument favoring Design 4 is its highest robustness to uncertainty among all the options considered, as shown by its CoV value.

As discussed in the section "Terminology," the proposed design approach focuses on maximum consequences, regardless of the occurrence probability of a fire. However, several design configurations that meet the performance objectives might be identified (Designs 2–5 in the current case study). Thus, additional performance metrics derived from the risk-based assessment of solutions obtained through the CFO approach could provide stakeholders with more comprehensive insights. These metrics can account for the occurrence probability of a vehicle fire underneath a bridge, enhancing decision-making capabilities.

Conclusions

This paper proposed a novel methodology for fire safety design under uncertainty, named the CFO approach. The main conclusions of this study are as follows:

- The fire–structure coupling effect unveils the possibility of designing structures that positively affect the combustion process and fire dynamics (and therefore define the hazard scenario). Differently, current approaches constrain the design to preliminarily selected scenarios that might not correspond to those maximizing fire impact.
- The proposed CFO approach enables exploiting the fire–structure coupling effect to optimize the balance between increasing structural capacity and decreasing fire intensity. In this process, fire scenarios are treated as design variables and obtained as outputs in combination with the maximum consequence potential. Monte Carlo sampling is applied to investigate the effect of uncertainty propagation from selected stochastic inputs.
- The CFO approach was demonstrated through the fire safety design of a simplified single-span steel-girder bridge subject to car fires. The analysis revealed that the fire scenario (fuel bed location, heat release rate curve, tandem system position) maximizing consequences strongly correlates to the structural features and cannot be set a priori. This fact highlights the importance of incorporating the fire–structure coupling effect in the design process. Design modifications in clearance, girder height, and flange width increased the girder capacity, reduced the lateral flame spread, and modified the heat transfer mechanism. Eventually, four design configurations complying with the performance objectives were identified.
- The selected designs were compared in terms of time to untenable conditions t_u (from 19.33 to 22.17 min), probability of this time being lower than the acceptance threshold (from 0.216 to 1.6×10^{-5}), total nondimensional cost (from 60.867 to 1.155), and robustness to uncertainties. The latter was quantified through the coefficient of variation of the t_u distribution and spanned from 0.019 to 0.38. Because different criteria favored distinct designs, the stakeholders must select their preferred solution.

The simplicity of fire and heat transfer models defines how much a designer can leverage the fire–structure coupling effect. Hence, the CFO approach emphasizes the benefits of developing and implementing models that accurately capture this coupling. Future research should extend the proposed methodology to more complex structures (e.g., tall buildings, cable-stayed bridges) and environments (e.g., closed compartments, tunnel interior), where several variables can be optimized to control the combustion process and fire dynamics. In these contexts, the CFO approach can guide the identification of modeling aspects that, when further refined, enable better exploitation of the coupling effect.

Appendix. Example Limitations

The scope of this appendix is to clarify the limitations of the simplified case study.

Design Variables

Choosing the bridge clearance H as a design variable requires careful consideration. Indeed, increasing H implies adjusting the abutment and the approach height, which in turn requires additional earthworks and a larger backfill material volume. Both these modifications are accounted for in the considered cost model. Hence, despite the higher C_I, it is assumed that stakeholders and designers might favor this design choice due to the potential for a lower total cost C_T.

Cost Model

The considered costs aim to provide a rough, reasonable estimate of the bridge collapse consequences and should not be used as definite or absolute values. Indirect costs are obtained from the work of Limongelli et al. (2018), who studied the consequences of bridge failure due to earthquakes. All the assumptions of this reference (e.g., bridge located on a road connecting a village to a hospital, 30-km diversion due to traffic interruption, traffic composition of 70% light vehicles) are maintained for illustrative purposes.

A further limitation of this example is its focus on the consequences of collapse. However, considerable indirect losses can also stem from traffic restrictions dictated by minor-to-moderate fire incidents; such events might not cause significant damage but still necessitate inspections and repairs.

Fire Model

For illustrative purposes, a car is considered as the fire source. The statistical analysis by Peris-Sayol et al. (2017) shows that previous car fires typically resulted in superficial to slight (i.e., repairable without replacing main structural elements) damage. In contrast, fuel-tanker fires induced more severe damage levels in past fire accidents. This is consistent with the events described in other bridge fire reviews (e.g., Garlock et al. 2012; Hu et al. 2021). Nevertheless, while a car-fire-induced bridge collapse is an extreme event, its consideration does not invalidate or diminish the presented methodology's applicability. For example, Franchini et al. (2023) applied the CFO approach to heavy goods vehicle fires. Future development should carefully consider fuel-tanker and pool fires.

The simplified fire model adopted in this paper does not account for some fire–structure interaction effects observed, for instance, in the Valencia bridge test (Alos-Moya et al. 2017). First, Alos-Moya et al. (2017) observed that the burning rate varied depending on the relative position of the fuel pan and the structure. Specifically, when the fuel pan was placed close to the abutment, the burning rate was reduced due to the decreased oxygen supply (averaging −17.3%). Conversely, when reducing the distance between the fuel pan and the deck (from 1.7 to 1.1 m), the heat feedback increased the burning rate by 18.7%. These percentages are computed to the theoretical values. In the other examined cases, variations ranged from 0.9% to 13.3%. Second, an increased gas temperature (and therefore heat flux) at the deck level was observed when the fuel pan was placed close to the abutments. This is due to the decreased mixing rate with ambient air (Drysdale 2011) and the Coandă effect increasing the height of flames adhering to a vertical surface (Alos-Moya et al. 2019).

Therefore, the fire–structure coupling effect discussed in the section "A Structure-Specific Hazard" is only exploited in its most straightforward realization, i.e., how the bridge clearance affects flame impingement, tilting, and lateral spread. Other effects (including radiative feedback) could, however, be captured through more advanced CFD models (e.g., Alos-Moya et al. 2019), which are outside the scope of this study.

Last, the impact of thermal-induced deflections on the heat flux, specifically the time-dependent proximity of girder sections to the fuel bed as they undergo heating, is disregarded.

Heat Transfer Model

The heat transfer to the steel girder is computed through a lumped capacitance method, which assumes a uniform temperature distribution across a specific cross section at a given time. Such an assumption is generally acceptable if the Biot number [$Bi = h_T(V/A)/k$, representing the relationship between the temperature gradients in the gas and the solid phases] is much smaller than 1 (Torero et al. 2017) (e.g., $Bi < 0.1$; Zhang and Usmani 2015; Lienhard and Lienhard 2020). Assuming a total heat transfer coefficient $h_T = 45\ \mathrm{W/m^2\,K}$ (e.g., Torero et al. 2017) and the lowest limit value for the thermal conductivity ($k = 27.3\ \mathrm{W/mK}$) [EN 1993-1-2 (CEN 2005b)], the Biot number of the cross sections listed in Table 7 varies between 0.029 and 0.037. Hence, the assumption is acceptable for the scope of this paper.

However, when steel I-girders that support concrete slabs are exposed to fire, a nonlinear thermal gradient typically forms (e.g., Payá-Zaforteza and Garlock 2012; Alos-Moya et al. 2014). This occurs because the temperature of the upper flange tends to be lower than that of the web and bottom flange. This temperature difference can be attributed to two factors (e.g., Alos-Moya et al. 2017; Aziz et al. 2015): first, the presence of the slab partially shields the upper flange and absorbs heat from it; second, the lower flange and web are generally more exposed to the heat flux from the fire. Furthermore, the temperature of the web is initially higher than that of the lower flange, primarily because of its smaller thickness (Saglik et al. 2022).

The nonlinear thermal gradient has two main effects: it causes additional mechanical stresses (Alos-Moya et al. 2014) and leads to asymmetric temperature-dependent mechanical properties throughout the cross section. Consequently, it is not evident whether the lumped thermal capacity assumption overestimates or underestimates the bearing capacity of the analyzed cross section. It is eventually observed that the considered case study might still be representative of an intermediate case between restraint expansion-dominated and gradient-dominated problems, where the two effects balance and yield low mechanical stresses (Sanad et al. 2000b).

Structural Model

Fig. 2 shows that the right side of the girder is free to expand in the horizontal direction. This boundary condition reflects the assumption that the expansion joints can accommodate the fire-induced thermal expansion (e.g., dictated by seismic design requirements or appropriate fire design). It is also observed that the maximum horizontal displacements for the design configurations and fire scenarios listed in Table 7 are less than 6 cm, which can be accommodated by conventional expansion joints (e.g., Parke and Hewson 2022). When performing more accurate analyses or examining fires involving other types of vehicles (e.g., fuel tankers), the maximum thermal expansion of the girders should be limited due to adjacent abutments or spans (Payá-Zaforteza and Garlock 2012). Indeed, the restraint caused by these elements can generate significant axial forces in the girder (e.g., Peris-Sayol et al. 2015b).

The considered traffic model from the Eurocode represents the most extreme traffic conditions (excluding special vehicles) that are commonly anticipated on the primary roadways throughout European nations [EN 1991-2 (CEN 2003)]. Such conditions might be overly severe in a real bridge fire safety design context, and appropriate combination factors or more advanced (and less conservative) traffic models should therefore be considered (e.g., OBrien et al. 2015; Camara et al. 2019).

A further limitation of the performed structural analyses regards the failure assessment. In determining t_u, this paper only considers the global failure of the girder. However, local phenomena such as web and flange buckling (e.g., Payá-Zaforteza and Garlock 2012; Alos-Moya et al. 2014) might control the failure mode of the bridge and should be considered in more advanced analyses.

Data Availability Statement

All data, models, or code that support the findings of this study are available from the corresponding author upon reasonable request.

Acknowledgments

The first author greatly acknowledges the financial support of the Maurice Franses Memorial Trust; University College London's Department of Civil, Environmental and Geomatic Engineering; and the Society for Fire Protection Engineering through a student research grant as part of the May 2022 grant cycle. He also thanks Dr. Augustin Guibaud from University College London for the insightful discussions and constructive feedback.

References

Ahrens, M. 2021. "US fire death rates by state." National Fire Protection Association (NFPA) Research. Accessed March 13, 2023. https://www.nfpa.org/News-and-Research/Data-research-and-tools/US-Fire-Problem/Fire-deaths-by-state.

Alipour, A., B. Shafei, and M. Shinozuka. 2011. "Performance evaluation of deteriorating highway bridges located in high seismic areas." *J. Bridge Eng.* 16 (5): 597–611. https://doi.org/10.1061/(ASCE)BE.1943-5592.0000197.

Alos-Moya, J., I. Paya-Zaforteza, M. E. M. Garlock, E. Loma-Ossorio, D. Schiffner, and A. Hospitaler. 2014. "Analysis of a bridge failure due to fire using computational fluid dynamics and finite element models." *Eng. Struct.* 68 (Jun): 96–110. https://doi.org/10.1016/j.engstruct.2014.02.022.

Alos-Moya, J., I. Paya-Zaforteza, A. Hospitaler, and E. Loma-Ossorio. 2019. "Valencia bridge fire tests: Validation of simplified and advanced numerical approaches to model bridge fire scenarios." *Adv. Eng. Software* 128 (Feb): 55–68. https://doi.org/10.1016/j.advengsoft.2018.11.003.

Alos-Moya, J., I. Paya-Zaforteza, A. Hospitaler, and P. Rinaudo. 2017. "Valencia bridge fire tests: Experimental study of a composite bridge under fire." *J. Constr. Steel Res.* 138 (Nov): 538–554. https://doi.org/10.1016/j.jcsr.2017.08.008.

Attary, N., V. U. Unnikrishnan, J. W. van de Lindt, D. T. Cox, and A. R. Barbosa. 2017. "Performance-based tsunami engineering methodology for risk assessment of structures." *Eng. Struct.* 141 (Jun): 676–686. https://doi.org/10.1016/j.engstruct.2017.03.071.

Aziz, E. M., V. K. Kodur, J. D. Glassman, and M. E. M. Garlock. 2015. "Behavior of steel bridge girders under fire conditions." *J. Constr. Steel Res.* 106 (Jun): 11–22. https://doi.org/10.1016/j.jcsr.2014.12.001.

Babrauskas, V. 2016. "Heat release rates." In *SFPE handbook of fire protection engineering*, 799–904. New York: Springer.

Barbato, M., F. Petrini, V. U. Unnikrishnan, and M. Ciampoli. 2013. "Performance-based hurricane engineering (PBHE) framework." *Struct. Saf.* 45 (Nov): 24–35. https://doi.org/10.1016/j.strusafe.2013.07.002.

Beck, J. L., and K. M. Zuev. 2015. "Handbook of uncertainty quantification." In *Rare event simulation*. Berlin: Springer.

Beyler, C. 2016. "Fire hazard calculations for large, open hydrocarbon fires." In *SFPE handbook of fire protection engineering*, 2591–2663. New York: Springer.

Brushlinsky, N., S. Sokolov, P. Wagner, and B. Messerschmidt. 2022. "World fire statistics." Accessed May 8, 2023. https://www.ctif.org/sites/default/files/2022-08/CTIF_Report27_ESG_0.pdf.

BSI (British Standards Institution). 1987. *Fire tests on building materials and structures—Part 20: Method for determination of the fire resistance of elements of construction (general principles)*. BS 476-20. London: BSI.

Buchanan, A. H., and A. K. Abu. 2017. *Structural design for fire safety*. New York: Wiley.

Cadena, J., M. McLaggan, A. Osorio, J. Torero, and D. Lange. 2022. "Maximum allowable damage approach to fire safety performance quantification." *Fire Saf. J.* 128 (Mar): 103537. https://doi.org/10.1016/j.firesaf.2022.103537.

Cadena, J. E., A. F. Osorio, J. L. Torero, G. Reniers, and D. Lange. 2020. "Uncertainty-based decision-making in fire safety: Analyzing the alternatives." *J. Loss Prev. Process Ind.* 68 (Nov): 104288. https://doi.org/10.1016/j.jlp.2020.104288.

Camara, A., I. Kavrakov, K. Nguyen, and G. Morgenthal. 2019. "Complete framework of wind-vehicle-bridge interaction with random road surfaces." *J. Sound Vib.* 458 (13): 197–217. https://doi.org/10.1016/j.jsv.2019.06.020.

CEN (European Committee for Standardization). 2003. *Eurocode 1: Actions on structures—Part 2: Traffic loads on bridges*. EN 1991-2. Brussels, Belgium: CEN.

CEN (European Committee for Standardization). 2004a. *Eurocode 2: Design of concrete structures—Part 1-2: General rules - Structural fire design*. EN 1992-1-2. Brussels, Belgium: CEN.

CEN (European Committee for Standardization). 2004b. *Eurocode 5: Design of timber structures—Part 1-2: General—Structural fire design*. EN 1995-1-2. Brussels, Belgium: CEN.

CEN (European Committee for Standardization). 2005a. *Eurocode 3: Design of steel structures—Part 1-1: General rules and rules for buildings*. EN 1993-1-1. Brussels, Belgium: CEN.

CEN (European Committee for Standardization). 2005b. *Eurocode 3: Design of steel structures—Part 1-2: General rules—Structural fire design*. EN 1993-1-2. Brussels, Belgium: CEN.

Charlier, M., A. Gamba, X. Dai, S. Welch, O. Vassart, and J.-M. Franssen. 2021. "Modelling the influence of steel structure compartment geometry on travelling fires." *Proc. Inst. Civ. Eng. Struct. Build.* 174 (9): 739–748. https://doi.org/10.1680/jstbu.20.00073.

Clark, H. 2023. "Fire and rescue incident statistics. England, year ending September 2022: Data tables. Table 0501." Accessed March 14, 2023. https://www.gov.uk/government/statistics/fire-and-rescue-incident-statistics-england-year-ending-september-2022.

Clayton, C. R. I., R. I. Woods, A. J. Bond, and J. Milititsky. 2014. *Earth pressure and earth-retaining structures*. London: CRC Press.

Der Kiureghian, A., and O. Ditlevsen. 2009. "Aleatory or epistemic? Does it matter?" *Struct. Saf.* 31 (2): 105–112. https://doi.org/10.1016/j.strusafe.2008.06.020.

Devaney, S. 2015. "Development of software for reliability based design of steel framed structures in fire." Ph.D. thesis, School of Engineering, Univ. of Edinburgh.

Drysdale, D. 2011. *An introduction to fire dynamics*. Chichester, UK: Wiley.

Franchini, A., C. Galasso, and J. L. Torero. 2023. "Optimising the inherent fire capacity of structures." *Fire Saf. J.* 141 (Jun): 103883. https://doi.org/10.1016/j.firesaf.2023.103883.

Garlock, M., I. Paya-Zaforteza, V. Kodur, and L. Gu. 2012. "Fire hazard in bridges: Review, assessment and repair strategies." *Eng. Struct.* 35 (5): 89–98. https://doi.org/10.1016/j.engstruct.2011.11.002.

Gernay, T., N. Khorasani, and M. Garlock. 2016. "Fire fragility curves for steel buildings in a community context: A methodology." *Eng. Struct.* 113 (Jun): 259–276. https://doi.org/10.1016/j.engstruct.2016.01.043.

Gernay, T., and M. Salah Dimia. 2013. "Structural behaviour of concrete columns under natural fires." *Eng. Comput.* 30 (6): 854–872. https://doi.org/10.1108/EC-05-2012-0103.

Gritzo, L. A., and V. F. Nicolette. 1997. "Coupling of large fire phenomenon with object geometry and object thermal response." *J. Fire Sci.* 15 (6): 427–442. https://doi.org/10.1177/073490419701500601.

Hadjisophocleous, G. V., and J. R. Mehaffey. 2016. "Fire scenarios." In *SFPE handbook of fire protection engineering*, 1262–1288. New York: Springer.

Heskestad, G. 2016. "Fire plumes, flame height, and air entrainment." In *SFPE handbook of fire protection engineering*, 396–428. New York: Springer.

Heskestad, G., and T. Hamada. 1993. "Ceiling jets of strong fire plumes." *Fire Saf. J.* 21 (1): 69–82. https://doi.org/10.1016/0379-7112(93)90005-B.

Hu, J., R. Carvel, and A. Usmani. 2021. "Bridge fires in the 21st century: A literature review." *Fire Saf. J.* 126 (Dec): 103487. https://doi.org/10.1016/j.firesaf.2021.103487.

Hu, J., A. Usmani, A. Sanad, and R. Carvel. 2018. "Fire resistance of composite steel & concrete highway bridges." *J. Constr. Steel Res.* 148 (Jul): 707–719. https://doi.org/10.1016/j.jcsr.2018.06.021.

Hurley, M. J., and E. R. Rosenbaum. 2016. "Performance-based design." In *SFPE handbook of fire protection engineering*, 1233–1261. New York: Springer.

Iervolino, I., and C. Galasso. 2012. "Comparative assessment of load–resistance factor design of FRP-reinforced cross sections." *Constr. Build. Mater.* 34 (5): 151–161. https://doi.org/10.1016/j.conbuildmat.2012.02.021.

Ingason, H., S. Gustavsson, and M. Dahlberg. 1994. *Heat release rate measurements in tunnel fires*. Rep. No. 1994:08. Borås, Sweden: Swedish National Testing and Research Institute.

Jiang, J., L. Jiang, P. Kotsovinos, J. Zhang, A. Usmani, F. McKenna, and G.-Q. Li. 2015. "*OpenSees* software architecture for the analysis of structures in fire." *J. Comput. Civ. Eng.* 29 (1): 04014030. https://doi.org/10.1061/(ASCE)CP.1943-5487.0000305.

Jowsey, A. 2006. "Fire imposed heat fluxes for structural analysis." Ph.D. dissertation, BRE Centre for Fire Safety Engineering, Univ. of Edinburgh.

Kaplan, S., and B. J. Garrick. 1981. "On the quantitative definition of risk." *Risk Anal.* 1 (1): 11–27. https://doi.org/10.1111/j.1539-6924.1981.tb01350.x.

Karlsson, B., and J. G. Quintiere. 2022. *Enclosure fire dynamics*. London: CRC Press.

Kawagoe, K. 1958. *Fire behaviour in rooms*. Rep. No. 27. Tokyo: Building Research Institute.

Khan, A. A., A. Usmani, and J. L. Torero. 2021. "Evolution of fire models for estimating structural fire-resistance." *Fire Saf. J.* 124 (Sep): 103367. https://doi.org/10.1016/j.firesaf.2021.103367.

Kirchsteiger, C. 1999. "On the use of probabilistic and deterministic methods in risk analysis." *J. Loss Prev. Process Ind.* 12 (5): 399–419. https://doi.org/10.1016/S0950-4230(99)00012-1.

Kletz, T. A., and P. Amyotte. 2010. *Process plants: A handbook for inherently safer design*. London: CRC Press.

Kodur, V., E. Aziz, and M. Dwaikat. 2013. "Evaluating fire resistance of steel girders in bridges." *J. Bridge Eng.* 18 (7): 633–643. https://doi.org/10.1061/(ASCE)BE.1943-5592.0000412.

Kodur, V., P. Kumar, and M. M. Rafi. 2020. "Fire hazard in buildings: Review, assessment and strategies for improving fire safety." *PSU Res. Rev.* 4 (1): 1–23. https://doi.org/10.1108/PRR-12-2018-0033.

Kodur, V., and M. Z. Naser. 2021. "Fire hazard in transportation infrastructure: Review, assessment, and mitigation strategies." *Front. Struct. Civ. Eng.* 15 (Jun): 46–60. https://doi.org/10.1007/s11709-020-0676-6.

Lamont, S., A. S. Usmani, and M. Gillie. 2004. "Behaviour of a small composite steel frame structure in a 'long-cool' and a 'short-hot' fire." *Fire Saf. J.* 39 (5): 327–357. https://doi.org/10.1016/j.firesaf.2004.01.002.

Lange, D., S. Devaney, and A. Usmani. 2014. "An application of the peer performance based earthquake engineering framework to structures in fire." *Eng. Struct.* 66 (Jun): 100–115. https://doi.org/10.1016/j.engstruct.2014.01.052.

Lange, D., J. L. Torero, A. Osorio, N. Lobel, C. Maluk, J. P. Hidalgo, P. Johnson, M. Foley, and A. Brinson. 2021. "Identifying the attributes of a profession in the practice and regulation of fire safety engineering." *Fire Saf. J.* 121 (May): 103274. https://doi.org/10.1016/j.firesaf.2021.103274.

Lattimer, B. Y. 2016. "Heat transfer from fires to surfaces." In *SFPE handbook of fire protection engineering*, 745–798. New York: Springer.

Lienhard, J. H., IV, and J. H. Lienhard, V. 2020. *A heat transfer textbook*, 5th ed. Cambridge, MA: Phlogiston Press.

Limongelli, M. P., S. Miraglia, and A. Fathi. 2018. "The value of visual inspections for emergency management of bridges under seismic hazard." In *Proc., 6th Int. Symp. on Life-Cycle Civil Engineering Life-Cycle Analysis and Assessment in Civil Engineering: Towards an Integrated Vision*. London: CRC Press.

Ma, R., C. Cui, M. Ma, and A. Chen. 2019. "Performance-based design of bridge structures under vehicle-induced fire accidents: Basic framework and a case study." *Eng. Struct.* 197 (Jun): 109390. https://doi.org/10.1016/j.engstruct.2019.109390.

Mackie, K., and B. Stojadinovic. 2004. "Fragility curves for reinforced concrete highway overpass bridges." In *Proc., 13th World Conf. on Earthquake Engineering*. Tokyo: International Associations of Earthquake Engineering.

Maluk, C., M. Woodrow, and J. L. Torero. 2017. "The potential of integrating fire safety in modern building design." *Fire Saf. J.* 88 (Dec): 104–112. https://doi.org/10.1016/j.firesaf.2016.12.006.

Moehle, J., and G. G. Deierlein. 2004. "A framework methodology for performance-based earthquake engineering." In *Proc., 13th World Conf. on Earthquake Engineering*. Tokyo: International Associations of Earthquake Engineering.

Mohd Tohir, M. Z., and M. Spearpoint. 2013. "Distribution analysis of the fire severity characteristics of single passenger road vehicles using heat release rate data." *Fire Sci. Rev.* 2 (1): 5–26. https://doi.org/10.1186/2193-0414-2-5.

Moses, F. 1977. "Structural system reliability and optimization." *Comput. Struct.* 7 (2): 283–290. https://doi.org/10.1016/0045-7949(77)90047-5.

NFPA (National Fire Protection Association). 2020. *Standard for road tunnels, bridges, and other limited access highways*. NFPA 502. Quincy, MA: NFPA.

OBrien, E. J., F. Schmidt, D. Hajializadeh, X.-Y. Zhou, B. Enright, C. C. Caprani, S. Wilson, and E. Sheils. 2015. "A review of probabilistic methods of assessment of load effects in bridges." *Struct. Saf.* 53 (Jun): 44–56. https://doi.org/10.1016/j.strusafe.2015.01.002.

Parke, G., and N. Hewson. 2022. *ICE manual of bridge engineering*. London: Thomas Telford.

Paté-Cornell, M. E. 1996. "Uncertainties in risk analysis: Six levels of treatment." *Reliab. Eng. Syst. Saf.* 54 (2–3): 95–111. https://doi.org/10.1016/S0951-8320(96)00067-1.

Payá-Zaforteza, I., and M. E. M. Garlock. 2012. "A numerical investigation on the fire response of a steel girder bridge." *J. Constr. Steel Res.* 75 (Apr): 93–103. https://doi.org/10.1016/j.jcsr.2012.03.012.

Peris-Sayol, G., S. Balasch-Parisi, I. Paya-Zaforteza, and J. Alós-Moya. 2016. "Analysis of the factors that influence the maximum adiabatic temperatures in I-girder bridges." In *Proc., 9th Int. Conf. on Structure in Fire 2016*, 8–10. Princeton, NJ: Princeton Univ.

Peris-Sayol, G., I. Paya-Zaforteza, J. Alos-Moya, and A. Hospitaler. 2015b. "Analysis of the influence of structural models in fire responses of steel girder bridges." In *Proc., Structures Congress 2015*, 160–171. Reston, VA: ASCE.

Peris-Sayol, G., I. Paya-Zaforteza, J. Alós-Moya, and A. Hospitaler. 2015a. "Analysis of the influence of geometric, modeling and environmental parameters on the fire response of steel bridges subjected to realistic fire scenarios." *Comput. Struct.* 158: 333–345. https://doi.org/10.1016/j.compstruc.2015.06.003.

Peris-Sayol, G., I. Paya-Zaforteza, S. Balasch-Parisi, and J. Alós-Moya. 2017. "Detailed analysis of the causes of bridge fires and their associated damage levels." *J. Perform. Constr. Facil.* 31 (3): 103274. https://doi.org/10.1061/(ASCE)CF.1943-5509.0000977.

Petrini, F., and M. Ciampoli. 2012. "Performance-based wind design of tall buildings." *Struct. Infrastruct. Eng.* 8 (10): 954–966. https://doi.org/10.1080/15732479.2011.574815.

Porter, K. A. 2003. "An overview of peer's performance-based earthquake engineering methodology." In *Proc., 9th Int. Conf. on Applications of Statistics and Probability in Civil Engineering*. Rotterdam, Netherlands: Millpress.

Quiel, S. E., T. Yokoyama, L. S. Bregman, K. A. Mueller, and S. M. Marjanishvili. 2015. "A streamlined framework for calculating the response of steel-supported bridges to open-air tanker truck fires." *Fire Saf. J.* 73 (8): 63–75. https://doi.org/10.1016/j.firesaf.2015.03.004.

Saglik, H., A. Chen, and R. Ma. 2022. "Performance of bolted splice connection in i-girder composite bridges under tanker fire." *J. Constr. Steel Res.* 199 (Dec): 107590. https://doi.org/10.1016/j.jcsr.2022.107590.

Sanad, A. M., S. Lamont, A. S. Usmani, and J. M. Rotter. 2000a. "Structural behaviour in fire compartment under different heating regimes—Part 1 (slab thermal gradients)." *Fire Saf. J.* 35 (2): 99–116. https://doi.org/10.1016/S0379-7112(00)00024-2.

Sanad, A. M., S. Lamont, A. S. Usmani, and J. M. Rotter. 2000b. "Structural behaviour in fire compartment under different heating regimes—Part 2: (slab mean temperatures)." *Fire Saf. J.* 35 (2): 117–130. https://doi.org/10.1016/S0379-7112(00)00025-4.

Shaw, T., T. Gibson, J. Karlovšek, R. Emberley, and J. L. Torero. 2016. "Experimental evaluation of the heat flux induced by tunnel fires."

Tunnelling Underground Space Technol. 60 (Sep): 49–55. https://doi.org/10.1016/j.tust.2016.07.015.
Shrivastava, M., A. Abu, R. Dhakal, and P. Moss. 2019. "State-of-the-art of probabilistic performance based structural fire engineering." *J. Struct. Fire Eng.* 10 (2): 175–192. https://doi.org/10.1108/JSFE-02-2018-0005.
Thomas, P. H., A. J. M. Heselden, and M. Law. 1967. *Fully-developed compartment fires: Two kinds of behavior.* Norwich, UK: HM Stationery Office.
Tondini, N., A. Morbioli, O. Vassart, S. Lechêne, and J.-M. Franssen. 2016. "An integrated modelling strategy between a CFD and an FE software: Methodology and application to compartment fires." *J. Struct. Fire Eng.* 7 (3): 217–233. https://doi.org/10.1108/JSFE-09-2016-015.
Torero, J. L. 2006. "The risk imposed by fire to buildings and how to address it." In *Protection of civilian infrastructure from acts of terrorism*, 41–57. Berlin: Springer.
Torero, J. L. 2013a. "Scaling-up fire." *Proc. Combust. Inst.* 34 (1): 99–124. https://doi.org/10.1016/j.proci.2012.09.007.
Torero, J. L. 2013b. "Structures in fire or fires in structures? Assessing the true performance of structures in fire." In *Proc., 5th Int. Conf. on Structural Engineering, Mechanics and Computation*. Taylor & Francis: London.
Torero, J. L. 2019. "Fire safety of historical buildings: Principles and methodological approach." *Int. J. Archit. Heritage* 13 (7): 926–940. https://doi.org/10.1080/15583058.2019.1612484.
Torero, J. L., A. Law, and C. Maluk. 2017. "Defining the thermal boundary condition for protective structures in fire." *Eng. Struct.* 149 (Oct): 104–112. https://doi.org/10.1016/j.engstruct.2016.11.015.
Torero, J. L., A. H. Majdalani, C. Abecassis-Empis, and A. Cowlard. 2014. "Revisiting the compartment fire." *Fire Saf. Sci.* 11 (1): 28–45. https://doi.org/10.3801/IAFSS.FSS.11-28.
Van Coile, R., D. Hopkin, D. Lange, G. Jomaas, and L. Bisby. 2019. "The need for hierarchies of acceptance criteria for probabilistic risk assessments in fire engineering." *Fire Technol.* 55 (4): 1111–1146. https://doi.org/10.1007/s10694-018-0746-7.
Washington State DOT. 2022. *WSDOT bridge design manual*. M 23-50.21. Olympia, WA: Washington State Department of Transportation.
Washington State DOT. 2023. "Unit bid analysis." Accessed June 21, 2023. https://wsdot.wa.gov/engineering-standards/design-topics/engineering-applications/unit-bid-analysis.
Welty, J., G. L. Rorrer, and D. G. Foster. 2020. *Fundamentals of momentum, heat, and mass transfer.* New York: Wiley.
Whittaker, A., R. Hamburger, and M. Mahoney. 2003. "Performance-based engineering of buildings and infrastructure for extreme loadings." In *Proc., AISC-SINY Symposium on Resisting Blast and Progressive Collapse*. New York: AISC.
Zhang, C., and A. Usmani. 2015. "Heat transfer principles in thermal calculation of structures in fire." *Fire Saf. J.* 78 (Apr): 85–95. https://doi.org/10.1016/j.firesaf.2015.08.006.
Zhu, Z., S. E. Quiel, A. Carlton, K. A. Mueller, and S. M. Marjanishvili. 2020. "Performance-based prioritisation of fire protection for steel girder overpasses in a complex highway interchange." *Struct. Infrastruct. Eng.* 16 (3): 394–411. https://doi.org/10.1080/15732479.2019.1666884.
Zukoski, E. E., B. M. Cetegen, and T. Kubota. 1985. "Visible structure of buoyant diffusion flames." In *Proc., Symp. (Int.) on Combustion*, 361–366. New York: Elsevier.